Sobolev, A., and Shimizu, N., (1993). Ultra-depleted primary melt included in an olivine from the Mid-Atlantic Ridge. Nature, 363, 151-154.

Wallace, P. J., and Carmichael, I.S.E. (1992). Sulfur in basaltic magmas. Geochimica et Cosmochimica Acta, 56, 1863-1874.

Wallace, P.J., and Carmichael, I.S.E. (1994). S speciation in submarine basaltic glasses as determined by measurements of SKα X-ray wavelength shifts. American Mineralogist, 79, 161-167.

CHAPTER 3

DETERMINATION OF SULFUR SPECIATION AND OXIDATION STATE OF OLIVINE HOSTED MELT INCLUSIONS

Michael C. Rowe
Adam J.R. Kent
Roger L. Nielsen

This manuscript has been submitted to Chemical Geology

ABSTRACT

In order to better understand what controls sulfur speciation in melt inclusions, and how that pertains to the primary basaltic chemistry of the system, we have conducted a series of rehomogenization experiments on naturally quenched and crystalline olivine-hosted melt inclusions. Sulfur speciation was determined from S Kα peak shift measurements by electron microprobe on the experimentally heated inclusions as well as a series of naturally quenched inclusions, and matrix glasses.

Naturally quenched olivine-hosted melt inclusions record a similar but more variable sulfur speciation to matrix glasses, (up to 45-50% variation in S^{6+}/S_{total}). Much of this range can be attributed to the effect of degassing which may either increase or decrease the S^{6+}/S_{total}. In addition, hydrogen diffusion and Fe-loss can both result in an oxidation of melt inclusions. A slight increase in S^{6+}/S_{total} and oxidation state can also occur from crystallization of olivine on the host-inclusion boundary. Rehomogenization of melt inclusions can have different effects on the sulfur speciation under different conditions. Overheating (above the temperature of entrapment) of inclusions will result in a reduction of the inclusion and decrease in sulfate proportion. This is caused by the addition of ferrous iron from the host olivine. An increase in heating times should result in an oxidation of the inclusion generated by increased hydrogen diffusion out of the inclusion. However, results of experiments for heating times less than 30 minutes do not show a significant increase in sulfur oxidation. By taking these parameters into account, sulfur speciation and oxidation state of basaltic melt trapped within inclusions can be

accurately determined from both naturally quenched and rehomogenized olivine-hosted melt inclusions.

INTRODUCTION

An accurate and precise determination of sulfur speciation from melt inclusions can provide constraints on the sulfur solubility and oxidation state of magmas. As a dissolved species in magmas, sulfur dominantly exists as sulfide (S^{2-}) under reducing conditions, below the Fayalite-Magnetite-Quartz (FMQ) oxygen buffer, and sulfate (S^{6+}) under oxidizing conditions (>FMQ +2 log units; Carroll and Rutherford, 1988; Wallace and Carmichael, 1992). Recent work has also indicated that several other species including sulfite (S^{4+}) and other radical anions (S_2^-, S_3^-) may also be present in significant concentrations and that sulfite may be influential at oxidation states between FMQ and FMQ+2 (Metrich et al., 2002; Winther et al., 1998; Jugo et al., 2005a). Less is known, however, about the solubility and relative proportions of these other species in magmas. Sulfur solubility is strongly dependant on speciation and oxidation state, with nearly 10 times greater sulfur concentrations in basaltic magmas at high fO_2 and S^{6+}/S_{total} (Jugo et al., 2005b). The dependence of solubility on speciation therefore has significant implications for numerous igneous processes and is especially relevant for volatile budgets and fluxes in subduction zones, volcanic degassing and ore genesis (for example: Luhr, 1990; Imai et al., 1993; Hedenquist and Lowenstern, 1994; Wallace, 2003; de Hoog et al., 2004; Wallace, 2005).

Magmatic oxidation states, and therefore sulfur speciation can also be strongly influenced by processes such as assimilation, fractional crystallization, and degassing (Mathez, 1984; Carmichael and Ghiorso, 1986; 1990; Sato and Wright, 1966). Melt inclusions trapped within early crystallizing phases provide a means of preserving melt compositions prior to significant modification of the magma. Analysis of these inclusions may allow us to better understand the oxidation state of the magma prior to significant assimilation, crystallization and degassing. Electron microprobe determination of the relative proportions of sulfide (S^{2-}) and sulfate (S^{6+}) is based on the position of the sulfur Kα X-ray peak (Fig. 9; Carroll and Rutherford, 1988; Wallace and Carmichael, 1994; Mathews et al., 1999; Jugo et al., 2005a). This technique provides relatively rapid analysis (50-100min/sample) of small samples (~30μm) and is therefore ideal for application to melt inclusions. However, olivine-hosted melt inclusions provide additional complications due to the potential for post-entrapment modification of the oxidation state through re-equilibration with the host, closed system fractional crystallization, and hydrogen diffusion out of the melt inclusion and olivine (Cottrell et al., 2002; Hauri, 2002; Danyushevsky et al., 2000; 2002). In addition, melt inclusions from slowly cooled lavas often require rehomogenization due to the growth of daughter crystals within the inclusions and host mineral growth on the inclusion-host interface (Nielsen et al., 1998; Danyushevsky et al., 2002, Rowe et al., 2006). However, little is known about the effects of rehomogenization on oxidation state of the melt inclusion. Danyushevsky et al (2002) suggest that rehomogenization of inclusions, resulting in the melting of the host olivine, causes a reduction in the melt oxidation state due to the

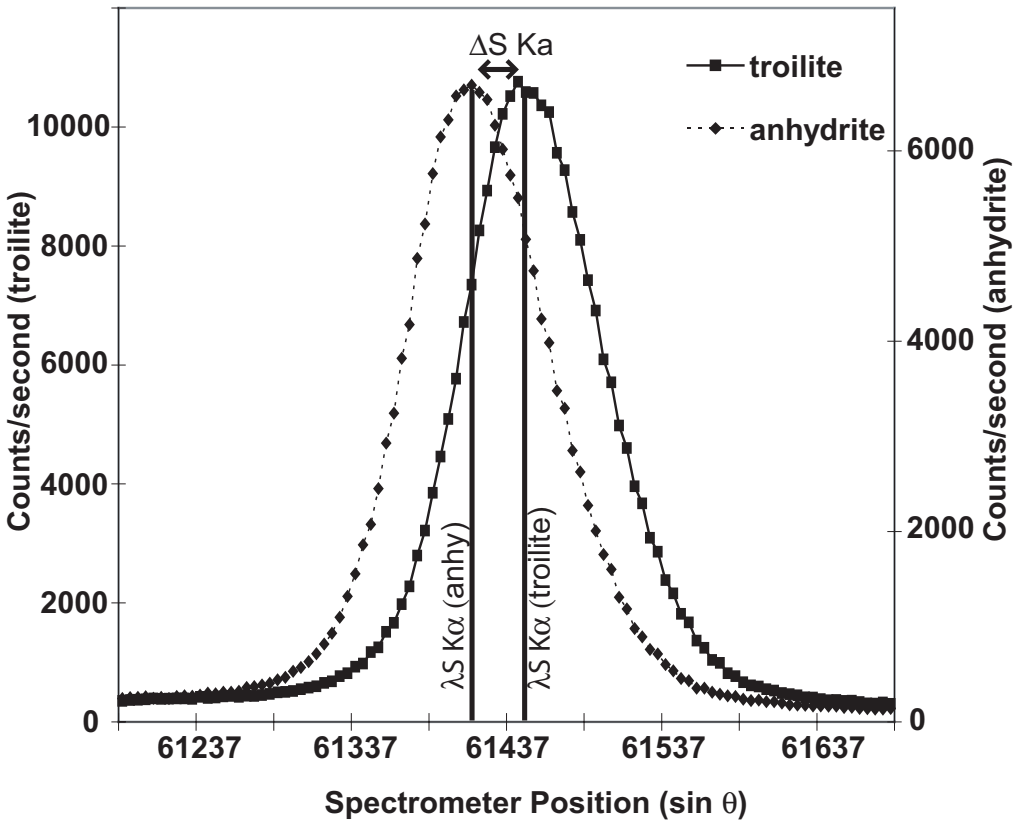

Figure 9. Wave scans of the SKα peak position for troilite and anhydrite standards. ΔS Kα shown here is the maximum possible shift (~3.0 Å*10^3) between sulfate (S^{6+}) and sulfide (S^{2-}).

increase in ferrous iron however direct measurement of this phenomena has not been previously attempted. Long heating times of rehomogenization may also result in the diffusion of hydrogen from the melt inclusion, causing oxidation of the melt (Hauri, 2002; Danyushevksy et al. 2002; Rowe et al., 2006).

This study addresses several analytical, experimental, and natural problems related to the determination of oxidation states and sulfur speciation in olivine-hosted melt inclusions. Through use of both naturally glassy melt inclusions and rehomogenized melt inclusions, we investigate the effects of hydrogen diffusion, magmatic degassing, olivine-melt re-equilibration, closed system fractional crystallization, and rehomogenization on melt sulfur speciation and oxidation state in basaltic melts. We show that with careful analysis and sample selection this technique provides reliable information on the sulfur speciation and oxidation state of the originally trapped melt.

SAMPLE DESCRIPTION

Five olivine-bearing basalts were selected for this study, two Oregon Cascade basalts and two Loihi pillow basalts and one Izu backarc basalt.

Loihi pillow basalt (LO-02-02; LO-02-04)

Loihi pillow lava samples LO-02-02 and LO-02-04 were collected by dredge 2 at a depth of 4200m during the 1989 Tunes IV expedition of the R/V Thomas Washington. Samples were dredged from the southern rift zone of Loihi seamount (18.77°N; 155.18°W; Kent et al., 1999a). LO-02-02 and LO-02-04 have similar modal mineralogy, glass inclusion and groundmass compositions and may be samples of the same flow

(Kent et al., 1999a). Naturally quenched, olivine-hosted glassy melt inclusions range from 9.71-11.57 wt% MgO as opposed to ~9 wt% MgO for the matrix glass. Reported olivine compositions range from $Fo_{86.0}$ to $Fo_{87.8}$ in LO-02-02.

Previous studies of Loihi basalt LO-02-02 and LO-02-04 (Kent et al., 1999a; Kent et al., 1999b) have presented evidence of significant assimilation of a seawater derived component resulting in matrix glass with major element compositions similar to those observed in melt inclusions but with high H_2O (1.56 wt%) and Cl (0.139 wt%). Melt inclusions from these samples cover a wide range of compositions. This was interpreted to represent the range of melts in the Loihi magmatic system prior to their aggregating and homogenizing in the magmatic conduit system (Kent et al., 1999a; Kent et al., 1999b)

Melt inclusions from LO-02-02, heated at 1200°C (at FMQ) for 15 minutes and 30 minutes have been previously analyzed for water loss during rehomogenization (A.J.R. Kent, unpublished data). Reanalyzing these melt inclusions for sulfur speciation allows us to 1) examine possible changes in the sulfur speciation as a function of heating time and 2) directly compare sulfur speciation and oxidation state with magmatic water content. In addition, by comparing sulfur speciation in the groundmass analyzed from LO-02-04, we can examine the effects of seawater assimilation on oxidation state by comparing the sulfur speciation in the matrix glass to the unheated melt inclusions.

Izu backarc basalt (31-7b)

Sample 31-7b is a submarine basalt collected from a backarc knoll in the Izu arc (lat 30.69°N; longitude 140.02°E). The basalt sample was collected during dredge 31 by

J. Gill and A. Hochstaedter (Hochstaedter et al., 2000). Major element concentrations for 31-7b are not available at this time however similar samples from the same dredge with comparable trace element concentrations (58.44ppm Ni, 142.12ppm Cr in 31-7b) suggest the sample has ~7 wt% MgO and ~50 wt% SiO_2 (J. Gill and D. Tollstrup, unpublished data). Olivine is the dominant phenocryst phase with lesser proportions of plagioclase and clinopyroxene.

Quartzville basalt (QV04-3b)

A sample from a young cinder cone in the Quartzville mining district in the western Oregon Cascades was used in order to expand the compositional range of the systems we examined. The sample is absarokitic, with high total alkalis (5.99 wt% Na_2O+K_2O) and 9.86 wt% MgO. The phenocryst assemblage is olivine ($Fo_{86.1-90.5}$) with minor clinopyroxene. Previous work on this basalt has indicated that it is oxidized (NNO +1; Rowe et al., 2006) relative to other contemporary basaltic lavas in the region. Sulfur concentrations in naturally quenched melt inclusions range from 2700 ppm to 5900 ppm. In addition, sufficient sulfur was retained in the scoria glass to allow for direct comparisons of sulfur speciation between naturally quenched melt inclusions and scoria glass from the subaerial eruption.

Cayuse Crater basalt (CC02-1)

Cayuse crater basalt flow, located in the Central Oregon High Cascades is a primitive calc-alkaline basalt (51.94 wt% SiO_2, 8.62 wt% MgO). Olivine is the only phenocryst phase present with plagioclase laths evident in the groundmass. Olivine phenocrysts have a compositional range of $Fo_{83.7}$ to $Fo_{88.3}$. Melt inclusions within this

subaerially erupted lava range from mostly glassy (>90% glass) to nearly completely crystalline. Due to an abundance of large melt inclusions with relatively constant major-element composition, this sample provided the best case for testing the affects of rehomogenization on a subaerially erupted basalt.

METHODS

Rehomogenization and analysis

Handpicked olivines were examined in ethanol to identify melt inclusion-bearing grains. Melt inclusions were heated/rehomogenized in a 1 atm Deltech vertical quench furnace. For heating experiments in this study we distinguish between samples which contain already glassy melt inclusions (referred to as heated), while melt inclusions which were crystalline prior to heating are referred to as rehomogenized.

A CO_2-H_2 gas mixture was utilized to regulate furnace atmosphere. Oxygen fugacity was maintained just below FMQ oxygen buffer for most runs, in order to inhibit magnetite crystallization (exception: one run of 31-7b olivines heated for 10 minutes at the IW oxygen buffer; Table 5). Except where specifically stated, rehomogenization/heating times have been kept to less than 15 minutes at temperatures above 1000°C and only 10 minutes at maximum temperature to reduce hydrogen diffusion in water-bearing melt inclusions (Hauri, 2002; Danyushevsky et al., 2002). Following the heating/rehomogenization, olivine grains were mounted in 1 inch epoxy rounds, or for small volume samples individually mounted, then polished and carbon-coated for microprobe analysis.

Table 5: Summary of heating experiments

Sample ID	Heating Time (min)	Temp. (°C)	MI (#)
31-7b	10	1143	3
31-7b[a]	10	1133	3
31-7b	20	1143	3
31-7b	30	1143	3
31-7b	10	1177	3
31-7b	10	1206	3
31-7b	10	1231	1
lo-02-02[b]	15	1200	3
lo-02-02[b]	30	1200	3
QV04-3b	10	1112-1119	2
CC02-1	15	1218-1224	6

Notes: [a]Rehomogenization conducted at the IW oxygen buffer (all other experiments at the FMQ oxygen buffer). [b]Rehomogenization performed by A.J.R. Kent (upd).

Glass inclusions, groundmass, and olivine grains were analyzed by electron microprobe on a Cameca SX100 at Oregon State University for major elements (and S and Cl for the glasses). Inclusions used in this study have a minimum diameter of 30 μm due to size limitations of the sulfur Kα peak shift technique. Melt inclusions were analyzed using a 7 μm, 30 nA beam with a 15 KeV accelerating voltage. A Makaopuhi Lava Lake basaltic glass (USNM 113498/1 VG-A99) was analyzed as an internal calibration standard while BCR-2G and LO-02-04 glasses were analyzed as external standards prior to each analytical session. It should be noted that sulfur concentrations reported by Kent et al (1999a) for LO-02-04 (700ppm) are significantly lower then the average value of multiple analyses performed at Oregon State University on a Cameca SX50 and Cameca SX100, which yielded sulfur concentrations of ~1400ppm. Sulfur concentrations reported by Kent et al (1999a) however are considered unreliable (A. Kent personal communication). Olivine grains were analyzed for major elements by electron microprobe using a 50 nA, 1 μm beam with a 15 KeV accelerating voltage. Springwater meteorite olivine (USNM 2566), was analyzed prior to each analytical session as an internal standard.

S Kα x-ray wavelength shifts

The SKα wavelength (λ[Skα]) shift analyses were conducted following the methods of Wallace and Carmichael (1994) and Carol and Rutherford (1988). Analyses were performed at Oregon State University on a Cameca SX100 electron microprobe and at the University of Oregon on a Cameca SX50 electron microprobe. SKα shifts were measured simultaneously on three PET crystals to determine the reproducibility of the

measurements. Anhydrite and pyrite were analyzed at the beginning of the analytical session and pyrrhotite and/or troilite was analyzed before and after every melt inclusion to correct for instrument drift. Beam conditions for sulfur peak shift measurements were similar to that used for glass major-element analysis with a 30 nA beam current, a 15 KeV accelerating voltage, and a 5-7 μm beam diameter. Each spectrometer was moved 0.00005 sin θ units for 100 steps with a 5 sec counting time for standards and 30 sec counting time ([S]>900 ppm) and 60 sec counting time ([S]<900 ppm) for unknowns at each step. Each wavelength scan was fitted with a Gaussian curve to determine the peak position of the scan, reported as λ(SKα). Even at counting times of 60 sec per step, errors in peak fitting become increasing problematic at S concentrations below 300 ppm. Wavelength shifts (ΔSKα) are reported relative to troilite (FeS) in units of angstroms times 1000 (reported as Å $*10^3$):

$$\Delta(SK\alpha)_{Unknown} = \lambda(SK\alpha)_{FeS} - \lambda(SK\alpha)_{Unknown} \qquad \text{equation (1)}$$

Several additional calculations are required to determine sulfur speciation (S^{6+}/S_{total}) and magmatic oxidation state (fO_2). Sulfur speciation is calculated relative to the peak shift of anhydrite, (assumed all S^{6+}), based on the following equation (Carroll and Rutherford, 1988).

$$S^{6+}/S_{total} = (\Delta(SK\alpha)_{Unknown} / \Delta(SK\alpha)_{Anhydrite}) * 100 \qquad \text{equation (2)}$$

Wallace and Carmichael (1994) derived the following relationship to determine oxygen fugacity based on sulfur speciation:

$$\log\left(\frac{X_{S^{6+}}}{X_{S^{2-}}}\right) = a * \log fO_2 + b/T(K) + c \qquad \text{equation (3)}$$

Where a=1.02, b=25410, and c=-10

Which when rearranged, solved for mole fraction sulfate, and referenced to the FMQ oxygen buffer (Jugo et al., 2005a) is:

$$X_{S^{6+}} = \frac{1}{\left[1 + e^{(2.73 - 2.35\Delta FMQ)}\right]} \qquad \text{equation (4)}$$

Where $X(S^{6+})$ is the mole fraction of sulfate

It should be noted that equations 2-4 are based on the assumption that S^{6+} and S^{2-} are the only valence states of sulfur present. Recent XANES sulfur K-edge analyses have identified up to 16% sulfite as a component in oxidized magmatic glasses (Metrich et al., 2002). However, experiments on sulfur speciation at high fO_2 (+5 to +6 Δlog FMQ) indicate only the presence of sulfide and sulfate (Paris et al., 2001). Strictly speaking, when sulfite is presumed to be present, equation 2 should be referred to as a percent sulfate equivalent or mole fraction sulfate equivalent ($X[S^{6+}]$) after Winther et al. (1998)

and Jugo et al. (2005a). However, because we have no constraints on the relative proportion of sulfite, we hold with the more commonly used notation of S^{6+}/S_{total} as representing the relative proportion of sulfate in glass.

Previous sulfur peak shift studies have observed that oxidation of the sulfur in glass may occur with prolonged beam exposure (Wallace and Carmichael, 1994). We conducted sulfur peak shift measurements on a number of samples and standards for varying times to test whether we could reproduce this result, and create a correction for this phenomenon. In glasses it was observed that higher sulfur glasses (higher initial sulfate proportion) generally experienced less oxidation than lower sulfur glasses (Fig. 10). However, a time series analysis of troilite, anhydrite, and barite mineral standards suggest that sulfur concentration and initial oxidation state may not be the only factor in determining the magnitude of the peak shift as no peak shift was observed during long beam exposure for troilite or barite standards while a significant shift was observed for long times on the anhydrite standard. This may suggest that bond type and strength is also a factor influencing the sulfur oxidation resulting from beam exposure. Na^+ migration has been suggested as a cause of surface oxidation of glasses (Fialin et al., 2004), however, the low S glass (Fig. 10) experiences a greater oxidation with prolonged beam time despite a lower Na_2O wt%. To avoid an apparent increase in $\lambda(SK\alpha)$ from exposure to the electron beam, the beam location is moved incrementally at a rate of 1 μm/minute. This requires there to be ~50μm^2 of "fresh" glass to allow for complete analysis. Care was taken to avoid microprobe beam spots from major element measurements.

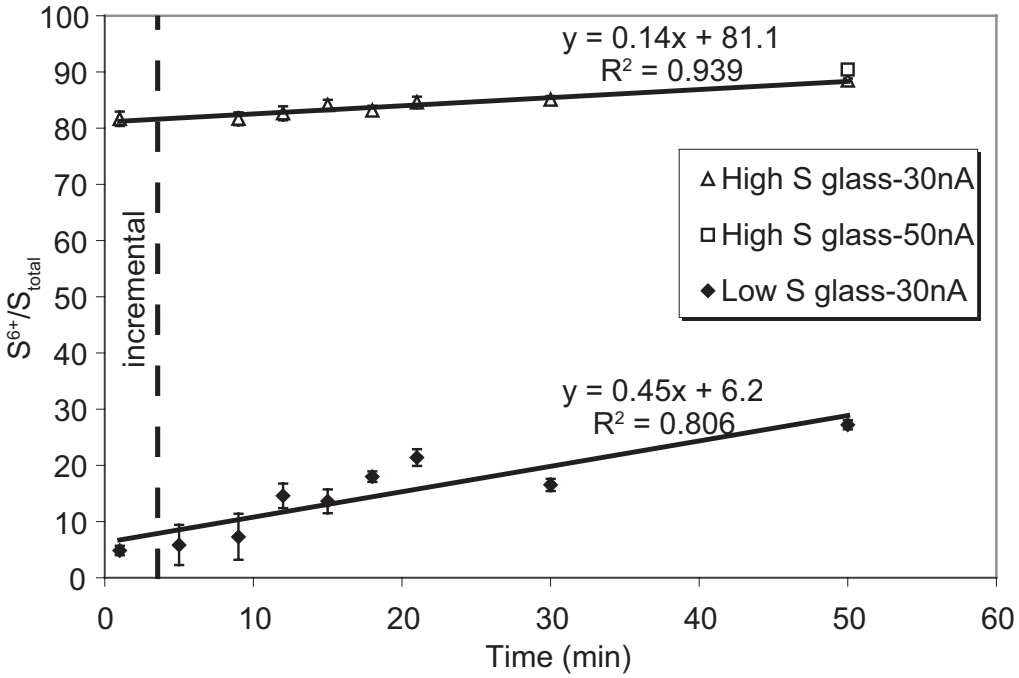

Figure 10. Increase in S^{6+}/S_{total} with increased beam exposure time for a high sulfur glass (2700ppm; QV04-3b) and low sulfur glass (1600ppm; K 14-3). One minute analyses were moved incrementally, 1μm/minute. Error bars on individual points are the average of the three spectrometer measurements (1 σ).

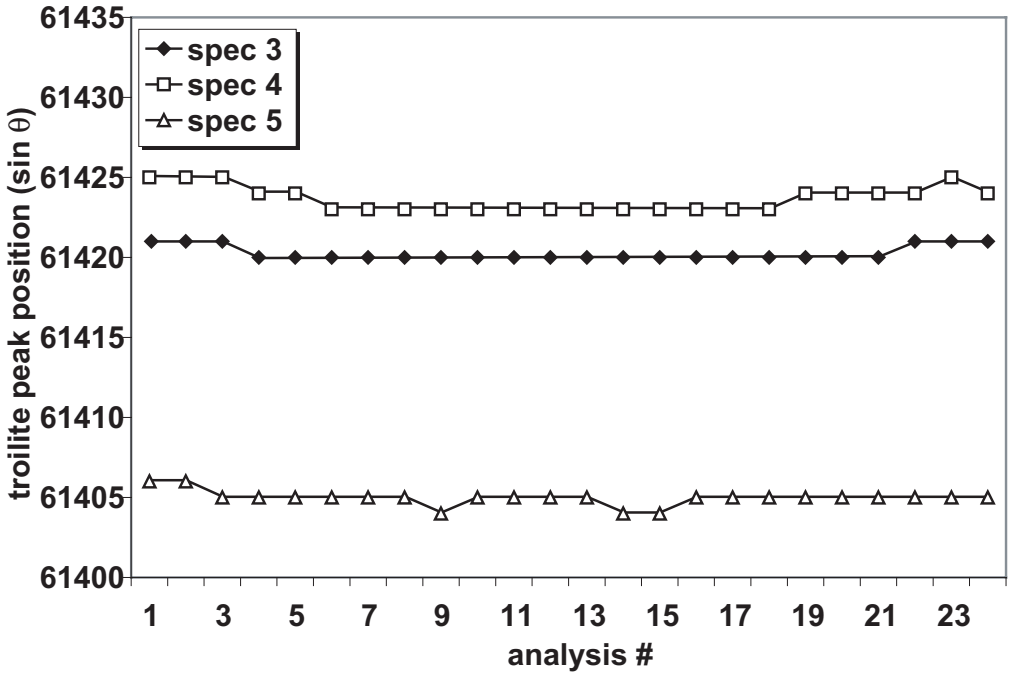

Figure 11. Peak positions determined for 24 analyses of the troilite standard over a 24 hour period for the three spectrometers. Peak positions calculated following the method described in the text. Error bars for the Gaussian peak fit (1 σ) are smaller than the symbol size.

Over the course of a 24 hour analytical session on the Cameca SX100 at Oregon State University, 24 troilite standard analyses were conducted (Fig. 11) to test the reproducibility of the peak position. The reproducibility of the peak position was 0.08 $Å*10^3$ for two spectrometers and 0.12 $Å*10^3$ for the third spectrometer (reported to 2 σ). Repeat analysis of a Galapagos Spreading Center (95.5°W) glass (K 14-3; Christie et al., 1986), using the glass analysis protocol with 30 second/step count times, reproduced the sulfur speciation to +/- 3.3% (1 σ based on 4 repeat analyses).

RESULTS

A total of 45 melt inclusions (12 naturally quenched, 33 reheated) were analyzed for major elements (including S and Cl) and sulfur speciation by electron microprobe (Table 6). Groundmass compositions and sulfur speciation results are reported for 31-7b, LO-02-04 (equivalent to LO-02-02), and QV04-3B. No glassy groundmass was available from CC02-1. Melt inclusion compositions have been re-calculated to be in equilibrium with their host olivine using the measured sulfur speciation and empirical curve defined by Wallace and Carmichael (1994) to determine the oxidation state and following procedures in Sobolev and Chaussidon (1996) and Rowe et al (2006). The empirical curve defined by Jugo et al. (2005a) is not utilized in this study to determine oxidation state. Although the Jugo et al (2005a) curve may prove to be more robust, taking into account the presence of sulfite, too few studies on the proportion of sulfite in oxidized magmas exist to for this to be well constrained at this time. Applying the oxygen fugacity and experimental temperatures to the Sack et al (1980) formulation, the

Table 6. Major elements and sulfur speciation of melt inclusions and glass.

Sample	31-7b							
ID	gm.3	25a	28a	1	15	26	10-3-1	10-4-1b
Temp ('C)	matrix	unheated	unheated	unheated	unheated	unheated	1143	1143
Time (min)							10	10
Measured melt inclusion compositions								
SiO_2	52.04	49.40	49.78	50.43	49.08	49.33	48.34	49.49
Al_2O_3	15.52	16.93	17.21	16.25	18.47	18.23	16.68	16.18
TiO_2	1.65	1.27	1.40	1.50	1.19	1.23	1.12	1.29
FeO[a]	11.34	10.24	10.05	10.51	9.40	9.22	9.65	10.70
MnO	0.19	0.18	0.16	0.17	0.16	0.14	0.17	0.17
CaO	10.50	11.53	11.29	11.68	12.11	12.25	11.61	10.50
MgO	5.64	6.18	5.54	5.29	6.28	5.66	7.53	7.22
K_2O	0.42	0.31	0.34	0.34	0.28	0.27	0.28	0.34
Na_2O	3.17	2.56	2.65	2.44	2.55	2.41	2.42	2.65
P_2O_5	0.23	0.23	0.21	0.22	0.18	0.20	0.23	0.19
S	0.029	0.119	0.098	0.109	0.167	0.156	0.172	0.115
Cl	0.084	0.061	0.072	0.076	0.054	0.058	0.056	0.070
H_2O[g]								
Total	100.84	98.99	98.81	99.02	99.92	99.15	98.26	98.97
S^{6+}/S_{total}	39.9	40.4	55.6	16.7	34.3	45.7	34.7	30.7
$\log fO_2$ (DFMQ)[b]	0.98	1	1.26	0.48	0.89	1.09	0.89	0.82
Host Fo #		0.82	0.81	0.82	0.82	0.83	0.83	0.83
$Kd_{ol\text{-}melt}$[c]		0.3	0.287	0.239	0.312	0.284	0.347	0.298
Adjusted melt inclusion compositions[d]								
SiO_2		49.40	49.68	49.96	49.15	49.23	48.67	49.48
Al_2O_3		16.93	17.06	15.57	18.62	18.05	17.26	16.16
TiO_2		1.27	1.39	1.44	1.20	1.22	1.16	1.29
FeO		8.31	8.00	9.18	7.68	7.51	7.81	9.01
Fe_2O_3		2.14	2.36	1.79	1.84	1.98	1.80	1.88
MnO		0.18	0.17	0.17	0.16	0.14	0.17	0.17
CaO		11.53	11.19	11.20	12.20	12.13	12.01	10.49
MgO		6.18	5.88	6.90	5.98	6.03	6.28	7.26
K_2O		0.31	0.33	0.32	0.29	0.27	0.29	0.34
Na_2O		2.56	2.63	2.33	2.57	2.39	2.51	2.65
P_2O_5		0.23	0.21	0.22	0.18	0.20	0.22	0.19
S		0.12	0.10	0.10	0.17	0.15	0.18	0.12
Cl		0.06	0.07	0.07	0.05	0.06	0.06	0.07
Total		99.20	99.06	99.28	100.10	99.35	98.41	99.16
$X_{olivine}$[f]		0.00	0.01	0.04	-0.01	0.01	-0.03	0.00

Notes:[a] FeO as total Fe. [b]log *f*O2 (DFMQ) determined from Wallace and Carmichael (1994). [c]$Kd_{ol\text{-}melt}$ determined from Sack et al (1981). [d]See text for detailed explanation of adjustment of melt inclusion compositions. [e]Experiments performed at the IW oxygen buffer (all other experiments performed at the FMQ oxygen buffer). [f]Fraction of olivine (by wt) added or subtracted from the melt composition.[g]H_2O determined by SIMS (A. Kent, upd; Kent et al. (2002)).

Table 6 (Continued)

Sample	31-7b							
ID	10-6-1	IW-4-2[e]	IW-6-1[e]	IW-1-1[e]	20-1-2b	20-3-1	20-6-1	30-2-1a
Temp ('C)	1143	1133	1133	1133	1143	1143	1143	1143
Time (min)	10	10	10	10	20	20	20	30
Measured melt inclusion compositions								
SiO_2	48.49	49.45	48.04	49.05	48.10	48.45	47.88	49.02
Al_2O_3	17.33	16.67	17.92	17.45	15.68	17.62	17.25	16.05
TiO_2	1.12	1.31	1.13	1.42	1.27	1.04	1.09	1.23
FeO[a]	8.64	10.40	8.55	9.72	11.99	9.04	8.99	9.80
MnO	0.19	0.18	0.18	0.18	0.23	0.16	0.17	0.17
CaO	11.61	11.07	11.82	10.98	11.07	11.65	11.61	10.69
MgO	7.64	6.87	6.82	7.29	6.88	7.64	7.75	7.51
K_2O	0.27	0.33	0.29	0.30	0.32	0.29	0.26	0.31
Na_2O	2.41	2.64	2.94	2.62	2.53	2.41	2.40	2.49
P_2O_5	0.17	0.20	0.19	0.25	0.21	0.19	0.14	0.21
S	0.162	0.133	0.122	0.158	0.113	0.177	0.172	0.086
Cl	0.054	0.067	0.060	0.067	0.066	0.062	0.057	0.067
H_2O[g]								
Total	98.16	99.36	98.18	99.53	98.47	98.75	97.79	97.68
S^{6+}/S_{total}	43.1	33.2	28.1	42.9	19.4	41.8	42.3	32.7
$\log f O_2$ (DFMQ)[b]	1.04	0.86	0.76	1.04	0.56	1.02	1.03	0.85
Host Fo #	0.84	0.80	0.84	0.82	0.81	0.84	0.83	0.82
$Kd_{ol\text{-}melt}$[c]	0.36	0.35	0.334	0.357	0.285	0.345	0.367	0.355
Adjusted melt inclusion compositions[d]								
SiO_2	48.90	49.81	48.26	49.43	47.98	48.75	48.33	49.44
Al_2O_3	18.09	17.25	18.34	18.15	15.50	18.22	18.10	16.70
TiO_2	1.16	1.36	1.16	1.48	1.26	1.07	1.15	1.28
FeO	6.85	8.15	6.84	7.51	10.34	7.29	7.10	7.93
Fe_2O_3	1.68	2.19	1.73	2.16	1.92	1.72	1.74	1.77
MnO	0.19	0.17	0.18	0.18	0.23	0.16	0.16	0.17
CaO	12.10	11.45	12.09	11.41	10.94	12.03	12.17	11.11
MgO	6.04	5.65	5.96	5.86	7.30	6.40	5.98	6.10
K_2O	0.28	0.34	0.30	0.31	0.31	0.30	0.28	0.32
Na_2O	2.52	2.73	3.01	2.72	2.50	2.49	2.51	2.59
P_2O_5	0.17	0.20	0.19	0.25	0.21	0.19	0.13	0.21
S	0.17	0.14	0.12	0.16	0.11	0.18	0.18	0.09
Cl	0.06	0.07	0.06	0.07	0.07	0.06	0.06	0.07
Total	98.22	99.55	98.32	99.76	98.65	98.89	97.92	97.83
$X_{olivine}$[f]	-0.04	-0.03	-0.02	-0.04	0.01	-0.03	-0.05	-0.04

Table 6 (Continued)

Sample	31-7b							
ID	30-6-1	30-1-1	1.1	1.2	2.1	1.2	2.1	3.1
Temp ('C)	1143	1143	1177	1177	1177	1206	1206	1206
Time (min)	30	30	10	10	10	10	10	10
Measured melt inclusion compositions								
SiO_2	49.46	48.61	48.09	47.89	48.47	48.39	48.07	47.09
Al_2O_3	18.22	15.01	15.45	16.20	16.07	14.90	15.03	14.35
TiO_2	1.20	1.27	1.07	1.09	1.13	1.16	1.02	1.01
FeO[a]	8.86	10.94	12.31	10.68	11.30	13.36	13.84	13.21
MnO	0.13	0.23	0.18	0.22	0.20	0.22	0.19	0.18
CaO	11.17	10.42	10.25	10.82	10.87	9.91	9.95	9.62
MgO	7.27	7.20	8.70	8.92	8.81	9.46	9.35	9.99
K_2O	0.30	0.35	0.28	0.27	0.24	0.29	0.26	0.26
Na_2O	2.72	2.67	2.40	2.34	2.35	2.50	2.32	2.12
P_2O_5	0.24	0.19	0.18	0.19	0.18	0.22	0.18	0.17
S	0.122	0.056	0.137	0.130	0.141	0.062	0.112	0.142
Cl	0.062	0.070	0.054	0.055	0.055	0.061	0.049	0.047
H_2O[g]								
Total	99.88	97.03	99.10	98.84	99.82	100.51	100.36	98.19
S^{6+}/S_{total}	27.6	30.1	41.1	27.9	22.9	34.7	16.2	27.6
$\log fO_2$ (DFMQ)[b]	0.75	0.8	1.01	0.76	0.65	0.89	0.46	0.75
Host Fo #	0.85	0.81	0.81	0.83	0.82	0.82	0.82	0.83
$Kd_{ol\text{-}melt}$[c]	0.301	0.333	0.36	0.37	0.365	0.328	0.299	0.332
Adjusted melt inclusion compositions[d]								
SiO_2	49.47	48.87	48.60	48.42	49.00	48.65	48.07	47.37
Al_2O_3	18.24	15.40	16.25	17.16	16.95	15.31	15.03	14.82
TiO_2	1.20	1.30	1.12	1.16	1.20	1.19	1.02	1.04
FeO	7.55	8.97	9.89	8.65	9.27	11.14	12.11	11.22
Fe_2O_3	1.45	2.01	2.38	1.88	1.90	2.35	1.92	2.10
MnO	0.13	0.23	0.17	0.22	0.19	0.22	0.19	0.17
CaO	11.18	10.68	10.76	11.45	11.45	10.17	9.95	9.93
MgO	7.24	6.32	6.99	6.86	6.93	8.51	9.35	8.92
K_2O	0.30	0.36	0.30	0.29	0.25	0.30	0.26	0.27
Na_2O	2.73	2.74	2.52	2.48	2.48	2.57	2.32	2.19
P_2O_5	0.24	0.18	0.17	0.19	0.18	0.21	0.18	0.17
S	0.12	0.06	0.14	0.14	0.15	0.06	0.11	0.15
Cl	0.06	0.07	0.06	0.06	0.06	0.06	0.05	0.05
Total	99.96	97.21	99.36	98.97	100.01	100.74	100.55	98.41
$X_{olivine}$[f]	0.00	-0.03	-0.05	-0.06	-0.05	-0.03	0.00	-0.03

Table 6 (Continued)

Sample	31-7b	LO-02-04	LO-02-02				
ID	3.1	lo-02-04ii	1	2	3	15xglass-A-1	15xcrystal-A-3
Temp ('C)	1231	matrix	unheated	unheated	unheated	1200	1200
Time (min)	10					15	15
Measured melt inclusion compositions							
SiO_2	47.82	49.30	47.55	47.92	48.41	48.47	47.49
Al_2O_3	14.60	12.17	12.44	12.42	12.38	11.49	11.66
TiO_2	1.02	2.24	3.16	3.14	2.87	2.13	2.79
FeO[a]	12.10	10.84	10.76	10.79	10.61	9.69	11.37
MnO	0.21	0.16	0.21	0.18	0.14	0.14	0.17
CaO	9.40	10.53	12.89	12.54	11.25	9.70	11.79
MgO	10.93	9.03	6.45	8.56	9.41	12.34	9.76
K_2O	0.27	0.59	0.58	0.37	0.60	0.55	0.37
Na_2O	2.25	2.48	1.99	1.87	1.88	1.86	1.96
P_2O_5	0.14	0.30	0.26	0.23	0.26	0.29	0.26
S	0.074	0.140	0.100	0.149	0.136	0.139	0.290
Cl	0.054	0.140	0.035	0.042	0.039	0.046	0.096
H_2O[g]		1.60				0.98	1.08
Total	98.87	99.52	96.43	98.21	97.99	97.84	99.09
S^{6+}/S_{total}	13.2	37.6, 44.9	23.9	22.8	17.3	35.6	28.2
log fO_2 (DFMQ)[b]	0.36	0.95, 1.07	0.67	0.64	0.5	0.91	0.76
Host Fo #	0.82		0.87	0.87	0.87	0.87	0.87
$Kd_{ol\text{-}melt}$[c]	0.391		0.195	0.249	0.268	0.401	0.269
Adjusted melt inclusion compositions[d]							
SiO_2	48.60		46.76	47.49	48.13	49.42	47.23
Al_2O_3	15.93		11.24	11.79	11.98	12.71	11.27
TiO_2	1.12		2.86	2.98	2.78	2.36	2.70
FeO	10.18		9.05	9.12	9.10	7.71	9.52
Fe_2O_3	1.68		2.05	1.94	1.73	1.91	2.08
MnO	0.21		0.21	0.18	0.14	0.14	0.17
CaO	10.24		11.64	11.90	10.88	10.71	11.40
MgO	7.97		10.29	10.53	10.66	8.75	11.01
K_2O	0.29		0.53	0.35	0.58	0.61	0.36
Na_2O	2.46		1.80	1.78	1.81	2.05	1.90
P_2O_5	0.13		0.23	0.22	0.26	0.29	0.26
S	0.08		0.09	0.14	0.13	0.15	0.28
Cl	0.06		0.03	0.04	0.04	0.05	0.09
Total	98.95		96.78	98.45	98.21	96.85	98.26
$X_{olivine}$[f]	-0.08		0.10	0.05	0.03	-0.10	0.03

Table 6 (Continued)

Sample	LO-02-02				QV04-3b		
ID	15xcrystal-B-2	30x-A-1	30x-B-1	30x-C-2	qvscoria	04-036-1	04-036-9
Temp ('C)	1200	1200	1200	1200	matrix	unheated	unheated
Time (min)	15	30	30	30			
Measured melt inclusion compositions							
SiO_2	47.56	48.58	47.73	46.32	50.61	50.33	50.05
Al_2O_3	10.48	11.65	11.24	11.39	16.74	14.80	15.55
TiO_2	2.20	2.59	2.71	2.61	1.74	1.65	1.79
FeO[a]	9.71	10.64	12.02	11.28	6.21	6.30	6.84
MnO	0.14	0.15	0.17	0.15	0.11	0.13	0.15
CaO	9.98	10.75	10.19	11.70	8.72	11.67	10.72
MgO	11.91	10.05	11.65	11.08	4.59	4.59	5.23
K_2O	0.43	0.46	0.38	0.33	3.40	2.38	1.34
Na_2O	2.16	1.85	1.70	1.84	3.91	2.77	3.05
P_2O_5	0.27	0.24	0.28	0.32	1.31	1.59	1.52
S	0.123	0.147	0.173	0.179	0.270	0.272	0.503
Cl	0.023	0.046	0.040	0.077	0.160	0.175	0.180
H_2O[g]	1.41	0.67	0.62	0.66			
Total	96.40	97.80	98.91	97.92	97.77	96.66	96.93
S^{6+}/S_{total}	31.5	30.6	17.6	17.6	67.9, 80.1	64.7	83.7
$\log f O_2$ (DFMQ)[b]	0.83	0.81	0.5	0.5	1.48, 1.75	1.42	1.86
Host Fo #	0.87	0.88	0.86	0.87		0.89	0.89
$Kd_{ol\text{-}melt}$[c]	0.38	0.288	0.315	0.307		0.276	0.244
Adjusted melt inclusion compositions[d]							
SiO_2	48.25	48.45	47.88	46.37		50.19	49.73
Al_2O_3	11.36	11.50	11.44	11.48		14.61	15.02
TiO_2	2.38	2.56	2.76	2.63		1.63	1.73
FeO	7.80	8.88	10.34	9.64		4.57	4.92
Fe_2O_3	1.92	1.97	1.85	1.82		2.01	2.28
MnO	0.14	0.15	0.17	0.15		0.13	0.15
CaO	10.80	10.61	10.37	11.79		11.53	10.36
MgO	9.02	10.51	11.02	10.80		5.13	6.71
K_2O	0.47	0.45	0.39	0.33		2.35	1.30
Na_2O	2.35	1.83	1.73	1.85		2.74	2.95
P_2O_5	0.27	0.24	0.28	0.32		1.58	1.48
S	0.13	0.14	0.18	0.18		0.27	0.49
Cl	0.02	0.05	0.04	0.08		0.17	0.17
Total	94.90	97.33	98.45	97.43		96.89	97.28
$X_{olivine}$[f]	-0.08	0.01	-0.02	-0.01		0.013	0.034

Table 6 (Continued)

Sample	QV04-3b				CC02-1
ID	04-050-17.1	04-050-20.1	05-014-1	05-014-7	03-015-26.1
Temp ('C)	unheated	unheated	1112-1119	1112-1119	1218-1224
Time (min)			10	10	15
Measured melt inclusion compositions					
SiO_2	50.18	50.34	49.39	49.05	50.87
Al_2O_3	15.67	15.35	17.10	17.00	17.43
TiO_2	1.89	1.87	1.81	1.82	1.04
FeO[a]	6.93	7.44	6.70	7.28	7.94
MnO	0.12	0.13	0.10	0.13	0.11
CaO	10.09	10.15	8.60	8.93	9.38
MgO	5.30	5.20	4.70	4.59	8.74
K_2O	1.55	1.85	4.23	4.00	0.66
Na_2O	2.58	1.63	3.54	3.50	3.21
P_2O_5	1.37	1.31	1.42	1.39	0.21
S	0.442	0.465	0.298	0.340	0.095
Cl	0.151	0.156	0.116	0.126	0.073
H_2O[g]					
Total	96.28	95.89	97.99	98.15	99.75
S^{6+}/S_{total}	75.8	86.6	58.1	72.5	31.2
$\log fO_2$ (DFMQ)[b]	1.65	1.96	1.3	1.57	0.83
Host Fo #	0.86	0.90	0.88	0.89	86.74
$Kd_{ol\text{-}melt}$[c]	0.305	0.208	0.241	0.195	0.365
Adjusted melt inclusion compositions[d]					
SiO_2	50.20	49.71	49.06	48.45	51.43
Al_2O_3	15.70	14.38	16.56	15.83	18.30
TiO_2	1.89	1.75	1.76	1.70	1.10
FeO	4.98	5.50	5.10	5.51	6.20
Fe_2O_3	2.14	2.34	1.90	2.20	1.66
MnO	0.12	0.13	0.10	0.13	0.11
CaO	10.11	9.52	8.37	8.33	9.85
MgO	5.21	7.94	6.07	7.54	6.84
K_2O	1.56	1.74	4.05	3.72	0.70
Na_2O	2.59	1.53	3.41	3.25	3.37
P_2O_5	1.37	1.24	1.50	1.31	0.21
S	0.44	0.44	0.28	0.32	0.10
Cl	0.15	0.15	0.11	0.12	0.08
Total	96.49	96.36	98.28	98.41	99.95
$X_{olivine}$[f]	-0.002	0.063	0.043	0.069	-0.048

Table 6 (Continued)

Sample	CC02-1				
ID	03-015-47.1	03-015-77.1	03-041-8.1	03-041-9.1	03-041-13.1
Temp ('C)	1218-1224	1218-1224	1218-1224	1218-1224	1218-1224
Time (min)	15	15	15	15	15
Measured melt inclusion compositions					
SiO_2	51.14	51.06	49.66	50.13	50.41
Al_2O_3	17.76	17.34	17.70	18.25	17.63
TiO_2	1.06	1.03	0.98	1.04	1.01
FeO[a]	8.04	7.29	8.51	7.71	7.70
MnO	0.13	0.13	0.15	0.10	0.13
CaO	10.06	10.10	9.65	9.92	9.80
MgO	8.90	9.41	8.03	8.24	8.66
K_2O	0.60	0.59	0.65	0.59	0.59
Na_2O	3.27	3.16	3.20	3.14	3.14
P_2O_5	0.19	0.17	0.22	0.23	0.25
S	0.110	0.104	0.112	0.089	0.111
Cl	0.053	0.049	0.056	0.056	0.055
H_2O[g]					
Total	101.31	100.44	98.91	99.49	99.48
S^{6+}/S_{total}	31.2	47.8	3.7	8.4	24.2
$\log f O_2$ (DFMQ)[b]	0.83	1.12	-0.22	0.14	0.68
Host Fo #	87.13	88.11	86.12	87.43	87.36
$Kd_{ol\text{-}melt}$[c]	0.355	0.382	0.294	0.310	0.350
Adjusted melt inclusion compositions[d]					
SiO_2	51.63	51.76	49.61	50.21	50.82
Al_2O_3	18.54	18.45	17.61	18.39	18.33
TiO_2	1.11	1.09	0.98	1.05	1.05
FeO	6.33	5.57	7.87	6.77	6.15
Fe_2O_3	1.69	1.62	0.74	1.01	1.54
MnO	0.13	0.13	0.15	0.10	0.13
CaO	10.49	10.73	9.60	10.00	10.18
MgO	7.22	6.95	8.22	7.93	7.16
K_2O	0.62	0.63	0.65	0.60	0.62
Na_2O	3.41	3.36	3.18	3.16	3.26
P_2O_5	0.19	0.17	0.22	0.23	0.26
S	0.11	0.11	0.11	0.09	0.12
Cl	0.05	0.05	0.06	0.06	0.06
Total	101.53	100.62	98.99	99.58	99.66
$X_{olivine}$[f]	-0.043	-0.060	-0.005	-0.001	-0.038

Fe^{2+}/Fe^{3+} is calculated for the melt inclusions. Assuming a constant olivine-melt Fe/Mg exchange of 0.3 the melt inclusion compositions can be numerically adjusted by incrementally adding or subtracting olivine from the melt composition (Table 6; Roedder and Emslie, 1970). Analytical results are summarized below for each of the four samples.

31-7b

Sulfur concentrations can be monitored in melt inclusions to determine if inclusions have degassed either naturally or during rehomogenization (Nielsen et al., 1998). Typically, inclusions which have sulfur concentrations significantly below the Fe-sulfide saturation curve defined by Wallace and Carmichael (1992) are assumed to be breached and therefore no longer reflect the initial trapped melt composition. At the highest reheating temperature (1231°C), melt inclusions have mostly degassed with only one inclusion maintaining high S (740ppm) and Cl (540ppm) concentrations. Sulfur concentrations vary from approximately 290 ppm in the groundmass to a maximum of 1720 ppm S in the melt inclusions at lower reheating temperatures (Table 6). Measured MgO content increases from 5.29-6.28 wt% in the naturally quenched inclusions to 10.93 wt% in the melt inclusion heated to 1231°C (Fig. 12a). This increase in measured MgO wt% is consistent with the melting of up to ~8 wt% olivine into the melt inclusion. S^{6+}/S_{total} in the naturally quenched inclusions range from 16.7 to 55.6%. S^{6+}/S_{total} in heated melt inclusions (at FMQ) varies from 30.7 to 43.1% at 1143°C down to 13.2% at 1231°C. Inclusions heated for 20 minutes and 30 minutes at the QFM oxygen buffer are statistically indistinguishable from those heated for 10 minutes, suggesting that heating

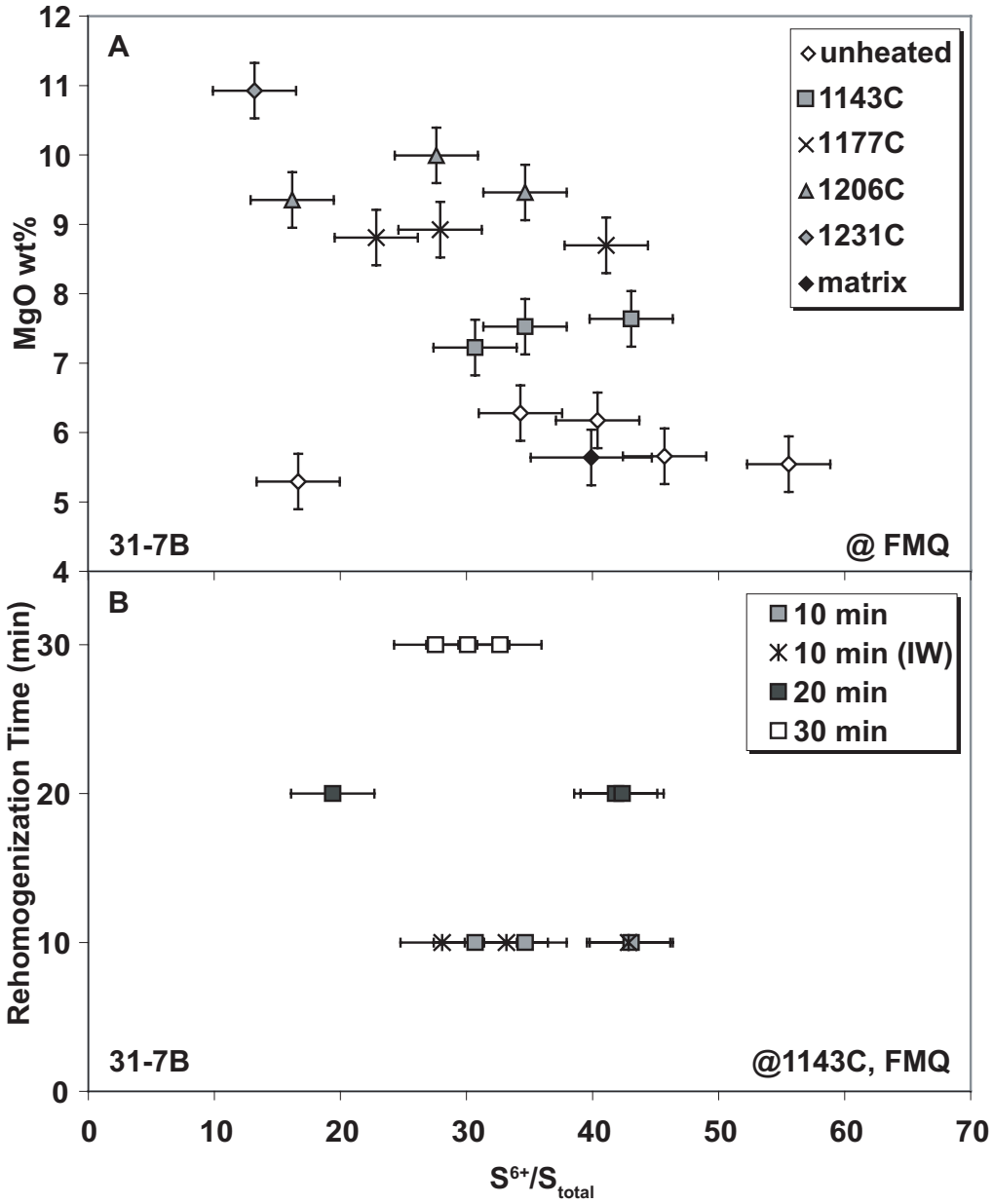

Figure 12. Reheating experiments for sample 31-7b. (a) Measured MgO wt% of inclusions reheated at constant time and oxygen fugacity (~FMQ) with variable temperature versus sulfur speciation. (b) Sulfur speciation of inclusions reheated at constant temperature with variable time. All heating experiments were conducted at the FMQ oxygen buffer except where specifically stated (i.e. IW). Error bars are 2 σ for sulfur concentrations, based on repeat analysis of LO-02-04ii, and 1 σ for sulfur speciation, determined by repeat analysis of glass K 14-3.

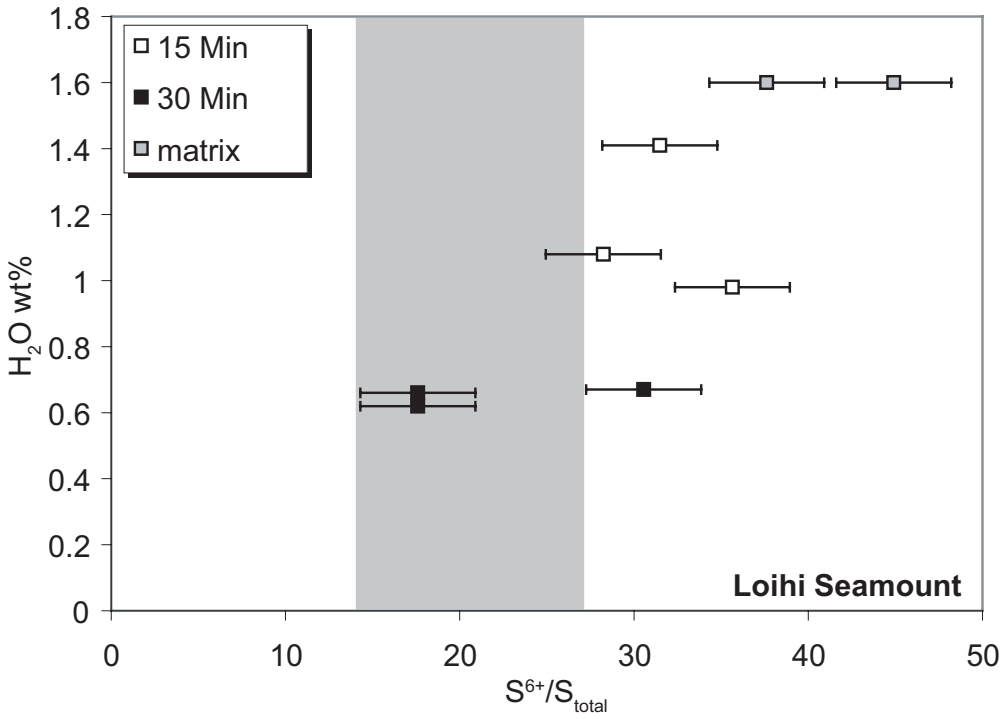

Figure 13. Sulfur speciation versus melt inclusion water content for LO-02-02. Also included are water contents and sulfur speciation measurements of LO-02-04 groundmass (see text). Grey field is the range of sulfur speciation observed in naturally quenched melt inclusions.

inclusions for 10-30 minutes does not cause significant changes in the sulfur speciation. In addition, inclusions heated for 10 minutes at 1133°C at the IW oxygen buffer are indistinguishable from those heated at FMQ (Fig. 12b).

LO-02-02

SIMS measurements of water concentrations in reheated inclusions range from 0.62 to 1.41 wt% H_2O, with groundmass water concentrations of 1.60 wt% H_2O (Kent et al., 1999a). In naturally quenched inclusions, S^{6+}/S_{total} ranges from 17.3 to 23.9, and 37.6 to 44.9% in the groundmass from sample LO-02-04. S^{6+}/S_{total} in reheated melt inclusions ranges from 17.6 to 35.6%. There is no systematic variation between sulfur speciation and the length of time the inclusions were reheated.

The small number of samples makes general conclusions difficult to draw, however, melt inclusions with higher S^{6+}/S_{total} (more oxidized) appear to correspond to high water concentrations in LO-02-02 (Fig. 13). However, despite clear evidence previously demonstrated by Kent et al (1999a) for assimilation of a seawater derived component based on Cl/K_2O ratios in naturally quenched melt inclusions and matrix glass there is no apparent systematic variation between Cl/K_2O ratios, ranging from 0.06 to 0.24, and sulfur speciation in the reheated melt inclusions.

QV04-3B

Naturally quenched and reheated melt inclusions from sample QV04-3B have sulfur concentrations ranging from 0.50 wt% S to 0.27 wt% S and chlorine ranging from 0.18 to 0.12 wt% Cl (Table 6). S^{6+}/S_{total} decreases from 86.6 to 58.1 percent sulfate, correlating with decreasing sulfur (Fig. 14), chlorine, and water (estimated by difference;

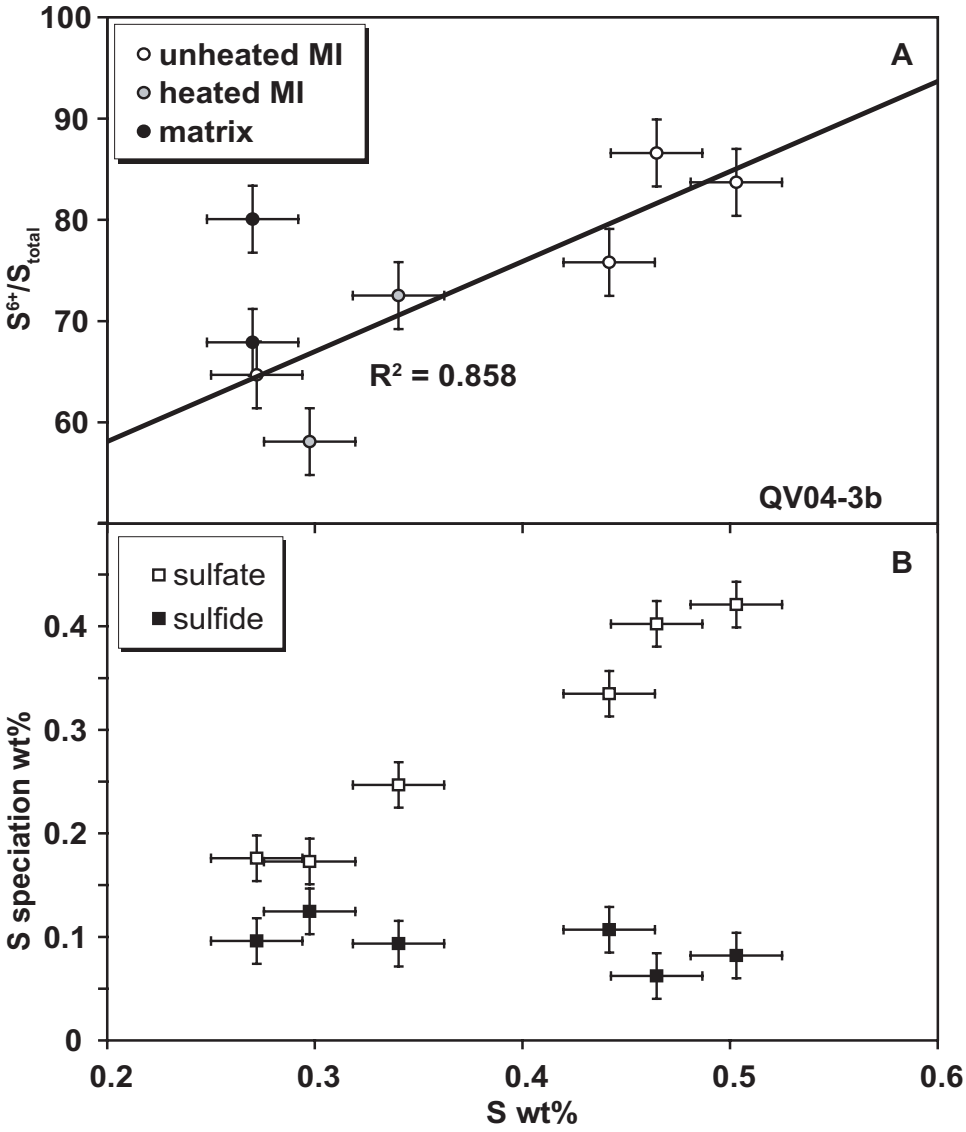

Figure 14. (a) Sulfur speciation versus total sulfur content for naturally quenched (open symbols) and reheated (grey symbols) melt inclusions and matrix glass (solid symbols) from sample QV04-3b. Error bars same as Figure 12. (b) Weight percent sulfide (solid symbols) and sulfate (open symbols) versus total sulfur concentration for QV04-3b reheated and naturally quenched melt inclusions. Error bars are 2 σ.

100-analytical total). Major element variation as a function of sulfur speciation is limited, with a weak negative correlation between S^{6+}/S_{total} and measured K_2O (4.23-1.34), Na_2O (3.54-1.63) and P_2O_5 (1.59-1.31).

Numerically corrected major element concentrations have the same trends as measured values however Al_2O_3 (negative) and MgO (positive) are also weakly correlated to S^{6+}/S_{total}. The observed decrease in volatile contents with relatively constant major element compositions suggests that the inclusions are recording varying degrees of degassing.

CC02-1

Six rehomogenized melt inclusions were analyzed for major elements and sulfur speciation from CC02-1. S^{6+}/S_{total} ranges from 3.7 to 47.8% in the rehomogenized melt inclusions. Both measured and adjusted melt inclusion compositions define clear correlations with percent sulfate (Fig. 15). Adjusted concentrations of SiO_2 (51.76-49.61), CaO (10.73-9.6), and Fe_2O_3 (1.62-0.74) have well defined positive correlations with sulfur speciation while Na_2O (3.41-3.16) and TiO_2 (1.11-0.98) have weak positive correlations. Adjusted MgO (8.22-6.95) and FeO (7.87-5.57) concentrations define negative correlations with sulfur speciation (Fig. 15).

DISCUSSION

In the following discussion, we demonstrate the variability of sulfur speciation as a result of both natural processes and inclusion rehomogenization. An important point for experiments such as are presented here is that melt inclusion modifications from fractional crystallization and melting, Fe-loss, and hydrogen diffusion can occur both

Figure 15. Major element variation (and Cl and S) as a function of sulfur speciation for sample CC02-1. Major elements have been numerically adjusted using the measured melt sulfur speciation to determine oxidation state and Fe^{2+}/Fe^{3+} after Sack et al. (1980). Error bars are same as Figure 12.

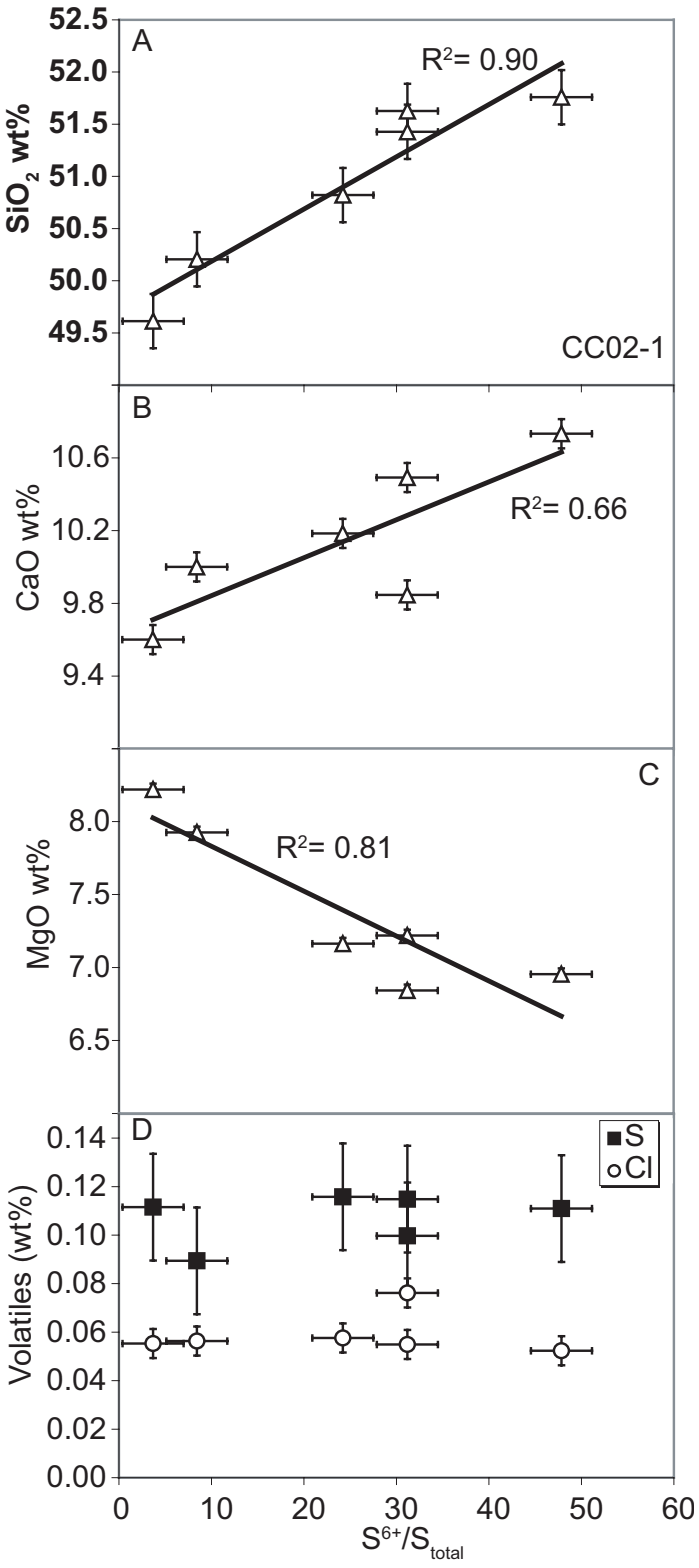
A
R²= 0.90
CC02-1
SiO2 wt%
52.5
52.0
51.5
51.0
50.5
50.0
49.5
B
R²= 0.66
CaO wt%
10.6
10.2
9.8
9.4
C
R²= 0.81
MgO wt%
8.0
7.5
7.0
6.5
D
S
Cl
Volatiles (wt%)
0.14
0.12
0.10
0.08
0.06
0.04
0.02
0.00
0
10
20
30
40
50
60
S6+/Stotal

Figure 15.

during natural magmatic processes and during rehomogenization. For the case of hydrogen diffusion, a potentially significant variable, we demonstrate the possible effects on sulfur speciation from reheating and as a result of natural processes, separately.

Inclusion v. matrix

It has been suggested that high sulfate proportions in primitive melt inclusions is largely the result of post-entrapment modification of melt inclusions (Metrich et al., 2005). To test this claim, the S^{6+}/S_{total} of olivine-hosted naturally glassy melt inclusions and coexisting glassy matrix material is compared for two samples, 31-7b, and QV04-3b. Melt inclusions correlate well with matrix glass measurements, however in general have a wider range in S^{6+}/S_{total} compared to matrix glass (Fig. 16).

There is a large discrepancy between S^{6+}/S_{total} from Loihi melt inclusions and matrix glass from sample LO-02-04. As was previously discussed, the high Cl/K and H_2O of the matrix glass has been interpreted as indicative of assimilation of a seawater derived brine in this lava (Kent et al., 1999a, Kent et al., 1999b). An additional consequence of this assimilation appears to also be an increase in the oxidation state of the matrix. The lower oxidation state (and percent sulfate) recorded by the naturally glassy inclusions suggests that they retain a S^{6+}/S_{total} of the melt prior to significant oxidation resulting from assimilation. Although the range exhibited in the inclusions from LO-02-02 can be attributed to varying amounts of assimilation, the wide range in sulfur speciation in naturally quenched melt inclusions from 31-7b and QV04-3b requires further examination.

Degassing

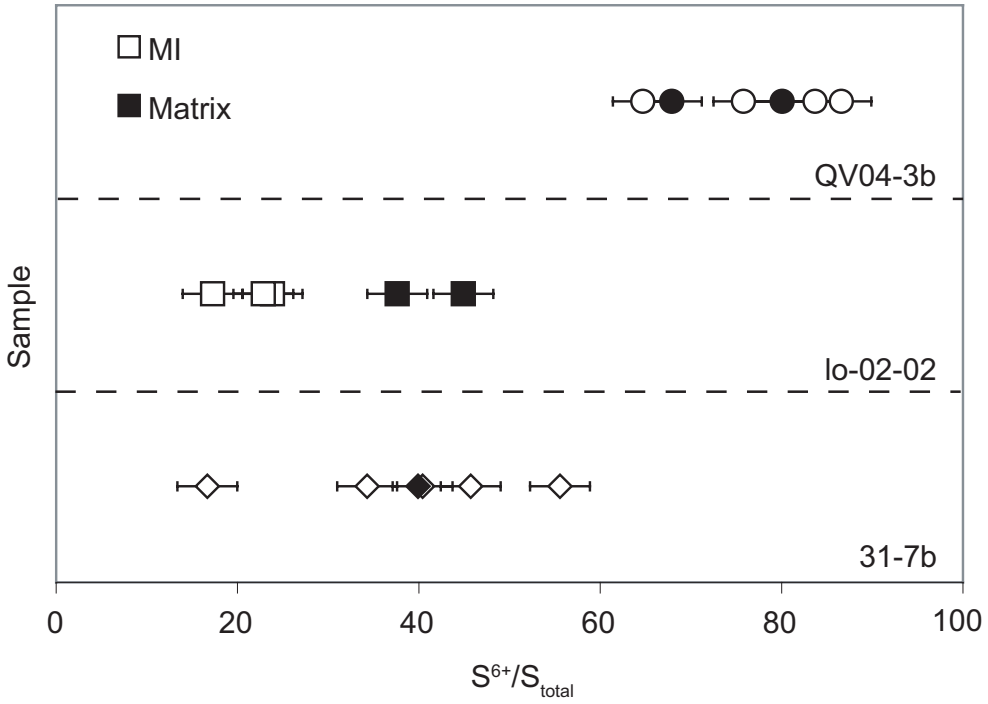

Figure 16. Sulfur speciation measured from both matrix glass and melt inclusions for three samples. Solid symbols are matrix glass and open symbols are melt inclusions. Note that in general melt inclusions depict a wider range in sulfur speciation than observed in the matrix glass. Error bars same as Figure 12.

Large ranges in measured sulfur speciation in naturally quenched melt inclusions may be related to degassing of the melt synchronous with entrapment in the olivine host crystals. 31-7b sulfur concentrations range downward from 1670ppm to 980ppm while S^{6+}/S_{total} increases from 34.3 to 55.6 (excluding one anomalously low point at S^{6+}/S_{total} of 10.6), suggesting the possibility that sulfide (S^{2-}) is preferentially lost during magmatic degassing (Table 5). Anderson and Wright (1972) and Wallace and Carmichael (1994) suggest that when SO_2/H_2S >>1, Fe is the oxidizing agent through the relationship:

$$S^{2-}_{(melt)} + 2Fe_2O_{3(melt)} = 4FeO_{(melt)} + SO_{2(gas)} \quad \text{(equation 5)}$$

In contrast, for sample QV04-3b there is a nearly 50% decrease in S concentration, from 5000ppm to 2700ppm S, with a decrease in S^{6+}/S_{total} (86.6-64.7) as sulfate is preferentially lost during degassing (Fig. 14b). Assuming Fe is the reducing agent for the sulfur in the melt, the following reaction likely describes this process:

$$SO^{2-}_{4(melt)} + 4FeO_{(melt)} = 2Fe_2O_{3(melt)} + SO_{2(gas)} \quad \text{(equation 6)}$$

These two samples illustrate a key challenge for tracking changes in magmatic oxidation state during degassing, in that the oxidation state of the gas phase does not necessarily coincide with the oxidation state of the melt, resulting in changing sulfur speciation as degassing progresses. In most basaltic magmas, SO_2 (sulfur as sulfite) is the dominant gas phase, although higher fH_2O can result in generation of H_2S as a dominant gas phase

(Carroll and Webster, 1994). However, we do not know how much of the S in SO_2 gas comes from oxidation of S^{2-} in the melt as opposed to the reduction of S^{6+} (P. Wallace, personal communication). Regardless, because they trap at high pressures, high sulfur melt inclusions suggest that they may provide the best estimate of magmatic oxidation states prior to significant degassing.

Fractional crystallization/melting

Closed system fractional crystallization has the potential to modify magmatic oxidation states by removal of ferrous iron (Fe^{2+}) through crystallization of early silicate phases (olivine and clinopyroxene). This will result in an increase in the system's Fe^{3+}/Fe^{2+} and oxidation state (Carmichael and Ghiorso, 1986). A similar process likely occurs in melt inclusions during cooling as the host mineral (in this case olivine) crystallizes on the mineral-inclusion boundary. As noted above, the heating experiments on sample 31-7b illustrate a decrease in oxidation state with increasing amount of olivine dissolution with progressive overheating in a closed system. If we examine those results in terms of progressive olivine addition and subtraction along the inclusion-olivine interface, assuming still a closed system, we can re-interpret our results in terms of fractional crystallization of olivine. In the case of 31-7b, there is a increase in S^{6+}/S_{total} from 13.2 to an average of 38.5% (+/- 13), or over a half a log unit increase in fO_2 relative to the FMQ buffer, corresponding to the crystallization of ~8 wt % olivine on the inclusion wall. Calculating the change in the Fe_2O_3/FeO ratio and oxidation state by simple addition of olivine to the melt, illustrates that this alone cannot generate the observed range in the Fe_2O_3/FeO ratio.

Starting with a naturally quenched melt inclusion from 31-7b (#15) and adding up to 13 wt% olivine to the melt (required to match the MgO of the experimental inclusion at 1231°C) produces a decrease in oxidation state relative to the FMQ oxygen buffer of only 0.13 log units, significantly lower than that determined from measurement of sulfur speciation. This result has two significant implications; 1) oxidation states of melt inclusions should not be significantly modified due to simple crystallization of the host mafic silicate mineral at the inclusion-host boundary, and 2) the larger variations in oxidation state of significantly overheated inclusions from sample 31-7b must be a result of other processes and may occur due to the rehomogenization of the inclusions (note also that the only inclusion from sample 31-7b at 1231°C has significantly lower S concentrations suggesting that some degassing may have occurred).

Rehomogenization conditions

Rehomogenization of melt inclusions can be a useful technique for determining glass compositions prior to significant degassing, assimilation or crystallization when naturally glassy melt inclusions are not available. However, little is known about the effects of inclusion rehomogenization on the oxidation state of melt inclusions. Knowledge of two important variables are essential for constraint of rehomogenization experiments; run time and temperature. It has been suggested that both processes may alter oxidation states of melt inclusions. It is important to recognize however that while we discuss these variables during rehomogenization the same principles apply to inclusions which reside at high temperatures for longer periods of time prior to eruption.

The first significant effect on inclusion oxidation state is a result of long times for rehomogenization. H_2 degassing was initially proposed by Sato and Wright (1966) as a method for changing magmatic oxidation states. H_2O dissociation and hydrogen in melt inclusions can produce a similar effect. Hauri (2002) demonstrated that hydrogen diffuses out of the inclusion and olivine host over realistic run times. The result of this diffusion is to provide excess O_2 in the inclusion, resulting in oxidation of the melt (Danyushevsky et al., 2002). Naturally glassy melt inclusions from samples LO-02-02 and 31-7b were reheated at near liquidus temperatures (1200°C and 1143°C, respectively) for 10-30 minutes (Fig. 12b). Although there is a slight decrease with time for sample LO-02-02 (35.6 to 17.6 % sulfate) this likely is a result of assimilation (see previous discussion). For sample 31-7b there is no increase in S^{6+} as a result of extended heating times, suggesting that at least at these temperatures, hydrogen diffusion does not significantly alter melt oxidation state when heating time is kept below 30 minutes.

Rehomogenization temperature may also have a significant effect on inclusion oxidation state, resulting as a function of the difference between the rehomogenization and trapping temperatures. As previously discussed fractional crystallization (and melting) to small degrees (<10 wt% of the host) will only have a slight effect on the melt oxidation state. Despite this, reheating experiments on 31-7b suggest that there is a much greater reducing effect on the melt inclusions than can be explained by fractional melting (Fig. 12a). At temperatures close to the melt liquidus there is no variation between melt inclusions reheated at the FMQ and IW oxygen buffers. However, this may not be the case at higher temperatures where the presence of H_2 gas in the furnace atmosphere may

begin to have a greater effect on the melt oxidation state. Since hydrogen diffuses relatively rapidly through both the melt and olivine host, at sufficiently high temperatures in the presence of a hydrogen-bearing atmosphere the melt inclusion may partially re-equilibrate with the furnace atmosphere (~FMQ) thus explaining the trend of melt oxidation state towards FMQ and the greater deviation from naturally quenched samples than could be explained by fractional melting (Fig. 12a). It should be reiterated however that at temperatures appropriate for reheating of inclusions in 31-7b there is no significant difference between the naturally quenched inclusions and those reheated at the FMQ and IW buffers despite the significantly greater volume of H_2 gas present in the furnace atmosphere at the IW oxygen buffer.

Hydrogen diffusion

Despite the results of relatively short duration heating experiments on LO-02-02 and 31-7b, the most likely inclusions to experience hydrogen diffusion are those which remain at high temperatures for extended periods of time (i.e. residing in a slowly cooling lava flow or in a magma chamber after entrapment). Sample CC02-1, in which melt inclusions were completely crystallized, illustrates the effects of hydrogen diffusion on the melt oxidation state. As previously depicted, despite constant S and Cl concentrations, there is a dramatic change in sulfur speciation and major element compositions exhibited in the population from CC02-1 melt inclusions (Fig. 15). In addition, at high S^{6+}/S_{total}, inclusions have the highest measured MgO wt% and the highest K_D (furthest out of equilibrium with the host olivine; Fig. 17). This would suggest that overheating had occurred resulting in too much olivine dissolution.

Figure 17. Measured (a) MgO wt% and (b) FeO wt%, and (c) olivine-melt K_D versus sulfur speciation for sample CC02-1. Olivine-melt K_D calculated based on Fe^{2+}/Fe^{3+} determination after Sack et al. (1980) with log fO_2 from sulfur speciation measurements. (d) Olivine correction (in wt%) required to adjust the melt composition to be in equilibrium with the host olivine assuming a K_D of 0.30 (Roedder and Emslie, 1970). Error bars for MgO and FeO wt% are 2 σ; sulfur speciation error same as previous figures.

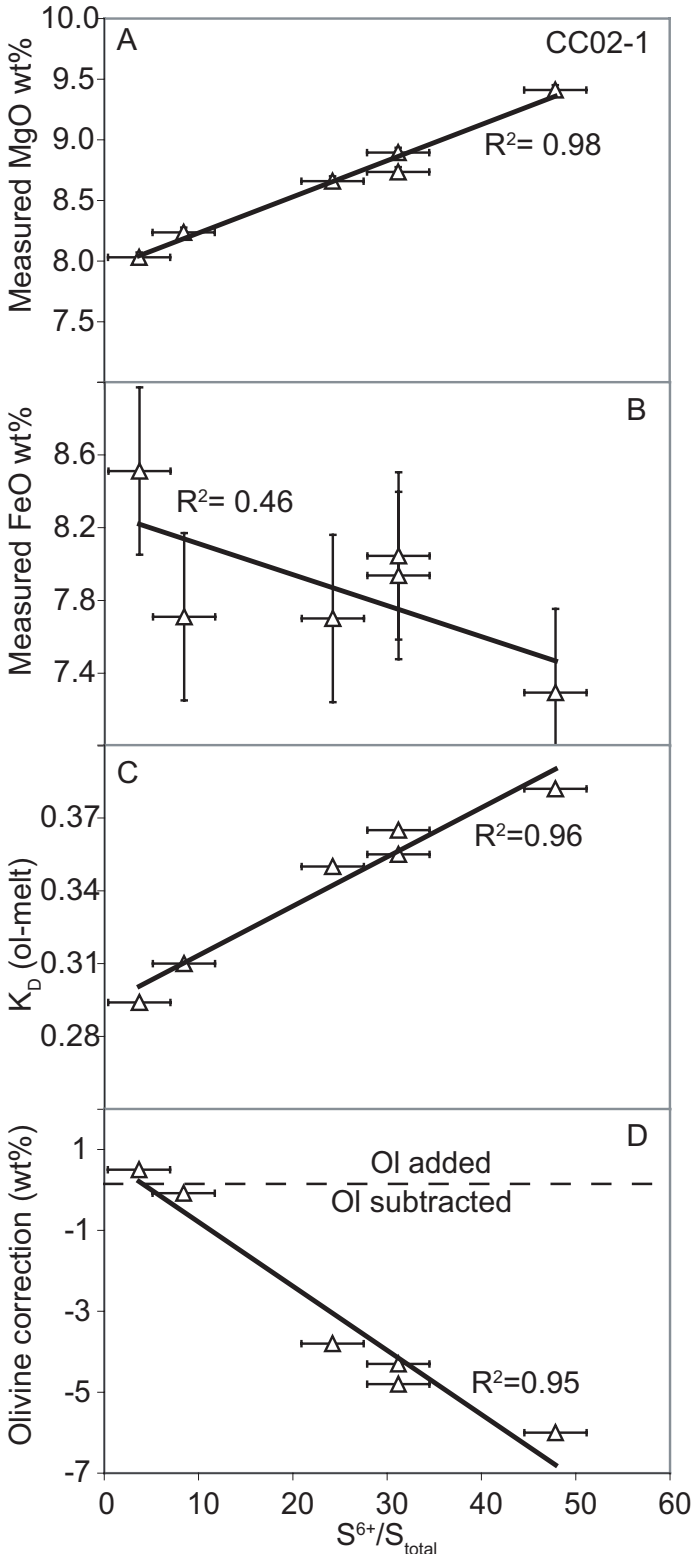
A
CC02-1
Measured MgO wt%
10.0
9.5
9.0
8.5
8.0
7.5
R2= 0.98
B
Measured FeO wt%
8.6
8.2
7.8
7.4
R2= 0.46
C
K_D (ol-melt)
0.37
0.34
0.31
0.28
R2=0.96
D
Olivine correction (wt%)
1
-1
-3
-5
-7
Ol added
Ol subtracted
R2=0.95
0
10
20
30
40
50
60
S6+/Stotal

Figure 17.

However, addition of olivine should result in a slight reduction of the basaltic melt rather than oxidation due to a decrease in $Fe^{+3}/(Fe^{+3}+Fe^{+2})$. The two most common methods for oxidizing melt inclusions are hydrogen diffusion and Fe-loss (Hauri, 2002; Danyushevksy et al., 2000). Fe-loss, resulting from re-equilibration of the host olivine, characteristically results in higher K_D values (>0.36) and Fe concentrations significantly lower than those of the whole rock. While several CC02-1 inclusions do have high K_D values the melt inclusion FeO* concentrations are equivalent to the host rock (7.85 wt%).

Two important observations support hydrogen diffusion as a likely cause for the range of values for sulfur speciation observed in CC02-1. First, if we assume that diffusion of hydrogen results in excess O_2 in the melt (Mathez, 1984) and that this oxygen results in the oxidation of Fe, then dissociation of only ~0.13 wt% H_2O followed by hydrogen diffusion, can cause the observed shift in oxidation state (increase of two log units) and the associated changes in sulfur speciation for this melt composition (Fig. 15, 17).

Second, melt inclusion compositions plotted in Figure 15 are numerically adjusted using the measured S^{6+}/S_{total} to estimate the oxygen fugacity. If the high S^{6+}/S_{total} measurements have been affected by post-entrapment hydrogen diffusion then this would likely explain the correlation between high sulfate percentages and high olivine-melt K_D's (up to 0.38). Taking the lowest measured sulfur speciation, which coincides with a melt-olivine K_D of 0.3, to be representative of all the inclusions then this oxidation state may be used to numerically recalculate the melt compositions. Following the same recalculation procedure with the new fO_2 estimate, compositional trends of the melt

inclusions as a function of S^{6+}/S_{total} disappear. These calculations suggest that the wide variation of oxidation state and sulfur speciation observed in CC02-1 is a result of hydrogen diffusion (post-entrapment modification) and does not reflect "real" variability in magmatic fO_2.

CONCLUSION

Despite complications with naturally quenched and reheated/rehomogenized melt inclusions, melt inclusions can provide reliable estimates of melt oxidation state at the time of inclusion entrapment. In naturally quenched melt inclusions, degassing and hydrogen diffusion have the greatest potential to alter melt oxidation states. While hydrogen diffusion out of the inclusion will result in oxidation of the melt, degassing may either oxidize or reduce the inclusion, depending on the initial melt oxidation state. Fractional crystallization (oxidation) or melting (reduction) may alter the melt oxidation state, albeit to a lesser extent. Fe-loss due to the re-equilibration of the inclusion and host may also result in an oxidation of the inclusion. Finally, our rehomogenization experiments have shown that at short experimental run times (~10 minutes) and temperatures that reproduce the original entrapment conditions, melt oxidation states can be accurately determined once other variables (degassing, hydrogen diffusion, crystallization, and Fe-loss) have been accounted for.

ACKNOWLEDGMENTS

The authors would like to thank Paul Wallace and John Donovan with initial sulfur speciation measurements and discussion and Frank Tepley for providing electron microprobe time at OSU. Thanks to Tom Sisson for discussing the possible effects of rehomogenization. Partial support for this study was provided by a Geological Society of America Student Research Grant and a Kleinman Grant through the USGS awarded to Michael Rowe and by Grant EAR 0440382 from the National Science Foundation.

REFERENCES

Anderson, A.T., and Wright, T.L. (1972). Phenocrysts and glass inclusions and their bearing on oxidation and mixing of basaltic magmas, Kilauea Volcano, Hawaii. American Mineralogist 57, 188-216.

Carmichael, I.S.E., and Ghiorso, M.S. (1986). Oxidation-reduction relations in basic magma: a case for homogenous equilibria. Earth and Planetary Science Letters 78, 200-210.

Carmichael, I.S.E., and Ghiorso, M.S. (1990). The effect of oxygen fugacity on the redox state of natural liquids and their crystallizing phases. In: Nicholls J., and Russel, J.K. (Eds.), Modern Methods of Igneous Petrology: Understanding Magmatic Processes. Reviews in Mineralogy 24, 191-212.

Carroll, M.R., and Rutherford, M.J. (1988). Sulfur speciation in hydrous experimental glasses of varying oxidation state: Results from measured wavelength shifts of sulfur X-rays. American Mineralogist 73, 845-849.

Carroll, M.R., and Webster, J.D. (1994). Solubilities of sulfur, noble gases, nitrogen, chlorine, and fluorine in magmas. In Carroll, M.R., and Holloway, J.R. (Eds.), Volatiles in Magmas. Reviews in Mineralogy 30, 231-279.

Christie, D.M., Carmichael, I.S.E., and Langmuir, C.H. (1986). Oxidation states of mid-ocean ridge basalt glasses. Earth and Planetary Science Letters 79, 397-411.

Cottrell, E., Spiegelman, M., and Langmuir, C.H. (2002). Consequences of diffusive reequilibration for the interpretation of melt inclusions. Geochemistry, Geophysics, Geosystems 3, 10.1029/2001GC000205.

Danyushevsky, L. V., Della-Pasqua, F.N., and Sokolov, S. (2000). Re-equilibration of melt inclusions trapped by magnesian olivine phenocrysts from subduction-related magmas: petrological implications. Contributions to Mineralogy and Petrology 138, 68-83.

Danyushevsky, L. V., McNeill, A.W., and Sobolev, A. (2002). Experimental and petrological studies of melt inclusions in phenocrysts from mantle-derived magmas: an overview of techniques, advantages and complications. Chemical Geology 183, 5-24.

De Hoog, J.C.M., Hattori, K.H., and Hoblitt, R.P. (2004). Oxidized sulfur-rich mafic magma at Mount Pinatubo, Philippines. Contributions to Mineralogy and Petrology 146, 750-761.

Fialin, M., Bezos, A., Wagner, C., Magnein, V., and Humler, E. (2004). Quantitative electron microprobe analysis of $Fe^{3+}/\Sigma Fe$: Basic concepts and experimental protocol for glasses. American Mineralogist 98, 654-662.

Hauri, E. H. (2002). SIMS analysis of volatiles in silicate glasses, 2: isotopes and abundances in Hawaiian melt inclusions. Chemical Geology 183, 115-141.

Hedenquist, J.W., and Lowenstern J.B. (1994). The role of magmas in the formation of hydrothermal ore deposits. Nature 370, 519-527.

Hochstaedter, A.G., Gill, J.B., Taylro, B., Ishizuka, O., Yuasa, M., and Morita, S. (2000). Across-arc geochemical trends in the Izu-Bonin arc: constraints on source composition and mantle melting. Journal of Geophysical Research 105, 495-512.

Imai, A., Listanco, E.L., and Fujii, T. (1993). Petrologic and sulfur isotopic significance of highly oxidized and sulfur-rich magma of Mt. Pinatubo, Philippines. Geology 21, 699-702.

Jugo, P.J., Luth, R.W., and Richards, J.P. (2005a). Experimental data on the speciation of sulfur as a function of oxygen fugacity in basaltic melts. Geochimica et Cosmochimica Acta 69, 497-503.

Jugo, P.J., Luth, R.W., and Richards, J.P. (2005b). An experimental study of the sulfur content in basaltic melts saturated with immiscible sulfide or sulfate liquids at 1300°C and 1.0 GPa. Journal of Petrology 46, 783-798.

Kent, A.J.R., Norman, M.D., Hutcheon, I.D., and Stolper, E.M. (1999a). Assimilation of seawater-derived components in an oceanic volcano: evidence from matrix glasses and glass inclusions from Loihi seamount, Hawaii. Chemical Geology 156, 299-319.

Kent, A.J.R., Clague, D.A., Honda, M., Stolper, E.M., Hutcheon, I.D., and Norman, M.D., (1999b). Widespread assimilation of a seawater-derived component at Loihi Seamount, Hawaii. Geochimica et Cosmochimica Acta 63, 2749-2761.

Luhr, J.F. (1990). Experimental phase relations of water- and sulfur-saturated arc magmas and the 1982 eruptions of El Chichon Volcano. Journal of Petrology 31, 1071-1114.

Mathez, E.A. (1984). Influence of degassing on oxidation states of basaltic magmas. Nature 310, 371-375.

Matthews, S.J., Moncrieff, D.H.S., and Carroll, M.R. (1999). Empirical calibration of the sulphur valence oxygen barometer from natural and experimental glasses: method and applications. Mineralogical Magazine 63, 421-431.

Metrich, N., Bonnin-Mosbah, M., Susini, J., Menez, B., and Galoisy, L. (2002). Presence of sulfite (S^{IV}) in arc magmas: Implications for volcanic sulfur emissions. Geophysical Research Letters 29, 10.1029/2001GL014607.

Metrich, N., Berry, A., O'Neill, H., and Susini, J. (2005). A XANES study of sulfur speciation in synthetic glasses and melt inclusions (abs): Geochimica et Cosmochimica Acta 69 (10) supplement 1, A51.

Nielsen, R.L., P. Michael, and Sours-Page, R. (1998). Chemical and physical indicators of compromised melt inclusions. Geochimica et Cosmochimica Acta 62, 831-839.

Paris, E., Giuli, G., and Carroll, M.R. (2001). The valence and speciation of sulfur in glasses by X-ray absorption spectroscopy. The Canadian Mineralogist 39, 331-339.

Roedder, E., and Emslie, R. (1970). Olivine-liquid equilibrium. Contributions to Mineralogy and Petrology 29, 275-289.

Rowe, M.C., Nielsen, R.L., and Kent, A.J.R. (2006). Anomalously high Fe contents in rehomogenized olivine hosted melt inclusions from oxidized magmas. American Mineralogist, 91, 82-91.

Sato, M., and Wright, T.L. (1966). Oxygen fugacities directly measured in magmatic gases. Science 153, 1103-1105.

Sack, R., Carmichael, I., Rivers, M., and Ghiroso, M. (1980). Ferric-ferrous equilibria in natural silicate liquids at 1 bar. Contributions to Mineralogy and Petrology 75, 369-376.

Sobolev, A. V., and Chaussidon, M. (1996). H_2O concentrations in primary melts from suprasubduction zones and mid-ocean ridges: Implications for H_2O storage and recycling in the mantle. Earth and Planetary Science Letters 137, 45-55.

Wallace, P. J., and Carmichael, I.S.E. (1992). Sulfur in basaltic magmas. Geochimica et Cosmochimica Acta 56, 1863-1874.

Wallace, P.J., and Carmichael, I.S.E. (1994). S speciation in submarine basaltic glasses as determined by measurements of SKα X-ray wavelength shifts. American Mineralogist 79, 161-167.

Wallace, P.J. (2003). From mantle to atmosphere: magma degassing, explosive eruptions, and volcanic volatile budgets. In: De Vivo, B., and Bodnar, R.J. (Eds.), Melt Inclusions in volcanic systems: methods, applications and problems. Developments in Volcanology 5, 105-127.

Wallace, P.J. (2005). Volatiles in subduction zone magmas: concentrations and fluxes based on melt inclusion and volcanic gas data. Journal of Volcanology and Geothermal Research 140, 217-240.

Winther, K.T., Watson, E.B, and Korenowski, G.M. (1998). Magmatic sulfur compounds and sulfur diffusion in albite melt at 1 GPa and 1300-1500°C. American Mineralogist 83, 1141-1151.

CHAPTER 4

ACROSS ARC VARIATION IN BASALTIC fO_2: INFLUENCE OF A SUBDUCTION COMPONENT IN THE CASCADIA SUBDUCTION ZONE

Michael C. Rowe
Roger L. Nielsen
Adam J.R. Kent

This manuscript is in preparation for submission to Journal of Petrology

ABSTRACT

Olivine-hosted melt inclusions from primitive basaltic lavas across the central Oregon Cascades (43°-45°N) have been analyzed for major-, trace- and volatile elements in an attempt to correlate basalt compositions to oxygen fugacity in a spatial context across the arc. Ocean island-like basalts and shoshonitic basalts have increasing concentrations of fluid-mobile trace elements closer to the trench. Low-K tholeiitic basalts and calc-alkaline basalts have little variation in trace element concentrations across the arc. Sulfur and Cl concentrations in melt inclusions are variable but reach concentrations of 0.6 wt% and 0.37 wt% respectively. High Cl concentrations in ocean island-like basalts appear to be anomalous and are interpreted to be the likely result of assimilation of a crustal brine.

Oxygen fugacity is determined in melt inclusions from sulfur speciation analyzed by electron microprobe and from olivine-chromite oxygen geobarometry. Olivine-chromite oxygen geobarometry has a smaller range in fO_2 compared to estimates from sulfur speciation and may be the result of sub-solidus re-equilibration. The overall range in fO_2 based on sulfur speciation measurements is from <-0.25 log units (ΔFMQ) to +1.9 log units (ΔFMQ). Sulfur oxidation and fO_2 increase proportional to increasing concentrations of fluid-mobile trace elements, with both generally increasing from backarc to arc to forearc. This correlation is interpreted to occur as a result of increased addition of a fluid-rich, oxidized subduction component closer to the trench. Estimates of the amount of subduction component (up to ~9.2 wt%) required to generate the geochemical diversity based on flux melt modeling correlate well with fO_2, with the

notable exception of calc-alkaline basalts which are more reduced than predicted from their trace-element concentrations. The lower fO_2 may result from re-equilibration with a low fO_2 mantle or lower crustal composition near the base of the crust. Low-K tholeiitic basalts, ocean island-like basalts, and shoshonitic basalts are interpreted to reflect the range in mantle source fO_2 in the subarc mantle, consistent with the range in fO_2 measured for mantle xenoliths from Simcoe volcano, WA.

INTRODUCTION

The oxidation state of the subarc mantle in subduction zones affects the phase equilibria and governs the transfer of multivalent trace elements (i.e. V, Eu, Cr) and speciation of volatile phases in primitive magmas. However, direct measurements of mantle oxygen fugacity in volcanic provinces is often limited to peridotite xenoliths entrained (i.e. Brandon and Draper, 1996; Parkinson and Arculus, 1999). Due to the rarity of such xenoliths in continental volcanic arcs broad generalizations of the subarc mantle fO_2 are often made on relatively limited data (Brandon and Draper, 1996). As a consequence, measured, calculated, and inferred oxidation states of primitive basalts have been widely used in an attempt to estimate differences in mantle source oxidation states (i.e. Ballhaus et al 1990; Ballhaus, 1993; Li and Lee, 2004; Christie et al., 1986; Arculus, 1985).

Most studies on the impact of partial melting, degassing and crystallization to basaltic oxygen fugacity have focused on ocean-island and mid-ocean ridge basalts (OIB and MORB, respectively) where melting and crystallization processes are typically

thought to be better constrained (Christie et al., 1986; Bezos and Humler, 2005). To the authors' knowledge no studies have quantified basaltic oxidation states, taking into account impact from addition of a subduction component and variable degrees of melting, in an attempt to put mantle source fO_2 variability into a spatial context across a subduction zone. The oxidation states of basalts may provide a reasonable measure of the relative differences in mantle oxidation state, despite the potential for modification resulting from processes such as partial melting, crystallization, assimilation, degassing and diffusion (Bezos and Humler, 2005; Mathez, 1984; Carmichael and Ghiorso, 1986; 1990; Sato and Wright, 1966). However, the magnitude to which the magma has been modified must be known if we are to use basaltic fO_2 to map out the range of oxidation states prevalent in the mantle, and to model how that correlates with other physical and chemical parameters of the system.

In subduction zones, as with other volcanic settings, basalt oxidation states may provide insight into the heterogeneity versus homogeneity of the mantle. Multiple compositionally distinct basaltic compositions are often observed in subduction zone magmatism. This diversity has been attributed to a number of variables including varying degrees of subduction-fluid induced flux melting (Stolper and Newman, 1994; Reiners et al., 2000; Walker et al., 2003) and/or mantle source heterogeneity (i.e. Leeman et al., 2005; Conrey et al., 1997; Bacon et al., 1997; Borg et al, 2002; Churikova et al., 2001; Hochstaedter et al., 2000). The addition of a subduction component (SC) to the subarc mantle has been demonstrated to exert significant control on the melting conditions and geochemical characteristics of the basaltic magmas (i.e. Hochstaedter et

al., 2001; Plank and Langmuir, 1993; Stolper and Newman, 1994). The subduction component is commonly interpreted as a fluid or hydrous silicate melt rich in incompatible, fluid-mobile elements (i.e. Cl, Ba, K, Na, La, Pb, Sr, U, Rb) derived from the dehydration or partial melting of the subducting oceanic plate and sediments (e.g. Stern, 2002; Schmidt and Poli, 1998; Tatsumi et al., 1986)

The goal of this study is to evaluate the effects of the addition of a subduction component to basaltic magmas by comparing variations in oxidation state with major-, trace- and volatile (S,Cl) element variability from distinct basalt groups across the central Oregon segment of the Cascade volcanic arc. In an attempt to reduce the impact of assimilation, degassing, and crystallization which can alter the oxidation state of the magma as well as its composition, we have focused the current study on primitive (whole rock >8 wt% MgO for the forearc and arc and >6 wt% MgO for the backarc), olivine-hosted ($Fo_{77-90.5}$) melt inclusions.

The Oregon Cascades, between 45-43°N are ideally suited for this detailed melt inclusion study. The study region has abundant olivine -phyric primitive basaltic and basaltic andesite flows and cinder cones, making this an exceptionally mafic segment of the Cascade volcanic arc (Fig. 18; Sherrod and Smith, 1990). Also, this is one of the few localities (along with southern Washington and northern California) in the Cascades where there is abundant, young (<1Ma) forearc and backarc volcanism, providing over 100 km of semi-continuous, coeval samples of basaltic magmatism across the arc (Guffanti and Weaver, 1988).

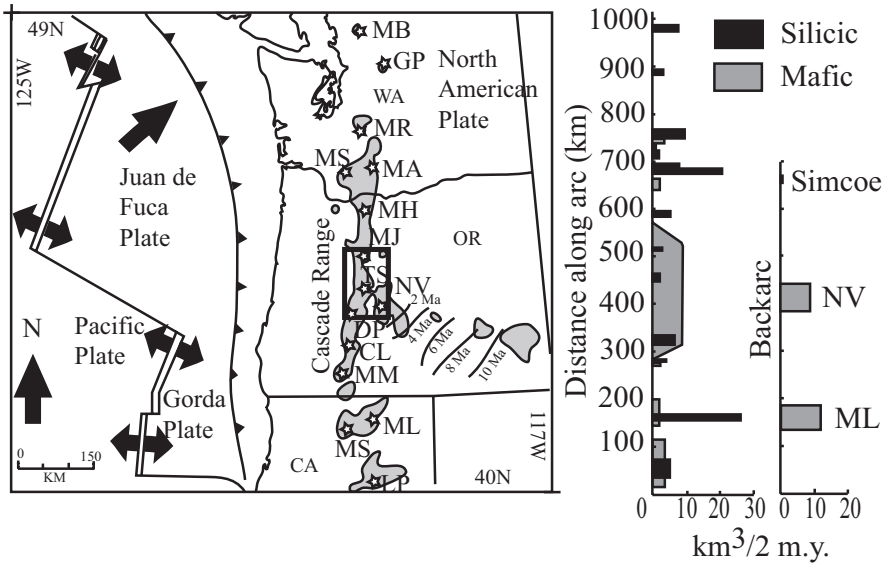

Figure 18: Location of study region from ~ 43-45 degrees N (bold outline). Major volcanic centers (stars) are (from N to S): Mt. Baker (MB), Garibaldi Pk. (GP), Mt. Rainier (MR), Mt. St. Helens (MS), Mt. Adams (MA), Mt. Hood (MH), Mt. Jefferson (MJ), Three Sisters (TS), Newberry Volcano (NV), Diamond Pk. (DP), Crater Lk. (CL), Mt. McLoughlin (MM), Mt. Shasta (MS), Medicine Lk. (ML), Lassen Pk. (LP). Shaded fields on map represent volcanic vents younger than 1 Ma (modified from Guffanti and Weaver, 1988). Graph illustrates the rate of mafic (grey) and silicic (black) volcanism along the Cascade arc (modified from Sherrod and Smith, 1990). Note the dramatic increase in mafic volcanism in the proposed study region and the presence of largely mafic back arc volcanism limited to Medicine Lake, Newberry Volcano, and Simcoe volcanic field (only mafic volcanism is plotted for backarc centers). Juan de Fuca plate motion vectors relative to North America from Riddihough (1984).

In addition to the geographic restrictions of this study (45-43°N) we have focused on basalts younger than 1 Ma (as identified by R. Conrey) to reduce potential variations in the subduction component, convergence rates, and thermal state of the subduction zone that may have influenced basalt petrogenesis over longer time intervals or along the arc. Detailed mapping and abundant whole-rock geochemical analyses of basaltic lavas within this region have led to the identification of young, compositionally diverse primitive lavas, providing a framework from which we have selectively targeted various primitive compositions for the present melt inclusion study (Conrey et al., 1997; 2002; Sherrod and Conrey, in prep; Sherrod et al., 2004; Jordan, 2001, Linneman, 1990; MacLeod and Sherrod, 1988; MacLeod and others, 1995; Higgins, 1973; Beyer, 1973).

OREGON CASCADES BACKGROUND

Tectonics and geophysics

The accretion of the Siletz terrane approximately 50 million years ago shifted the axis of volcanism in the Oregon Cascades to roughly its present N-S position, with an eastward migration of the volcanic front occurring in the last 10 million years (Fig. 18; Trehu, et al., 1994; Verplank and Duncan, 1987). The Juan de Fuca and Gorda plates are presently subducting beneath the North American Plate at a convergence angle of N50°E and a rate of 40 mm/yr (Verplank and Duncan, 1987). In addition, the close proximity of the Juan de Fuca spreading ridge to the convergent margin has resulted in the subduction of a young (~8 Ma), warm, thin oceanic plate (Stein and Stein, 1996).

Geophyiscal models suggest a wide range in slab dips resulting in large uncertainties for the relative position of the subducting slab beneath the volcanic front and backarc of the Oregon Cascades. Based on seismic tomography, Rasmussen and Humphreys (1988) have suggested that the subducting slab in the Oregon Cascade arc and backarc is dipping ~65° to the east, extending to a depth of 150 km whereas Harris et al. (1991) suggest a depth to the top of the Juan de Fuca plate of 100 km beneath the Cascades and 200 km beneath the backarc volcanism. Bostock et al. (2002) estimate the depth of the slab to be roughly 90 km beneath the arc and only 120 km beneath the backarc from S-wave perturbations. In contrast, density modeling based on observed gravity profiles suggest a much greater depth of 175 km to the top of the subducting slab beneath the Oregon Cascades and 250 km beneath the backarc (Romanyuk et al., 1998; 2001).

The Oregon segment of the Cascade volcanic arc is divided into two geographic provinces, the Western Cascades (40-10 Ma) and the High Cascades (10-0 Ma; Fig. 18). The high volume of mafic volcanism present in the central Oregon Cascades is largely the result of intra-arc rifting, estimated to have initiated approximately 5 million years ago near Three Sisters, OR in the High Cascades (Conrey et al., 2002; Sherrod and Smith, 1990). The northward propagation of the Cascade rift is likely related to the infringement of Basin and Range extension into the volcanic arc and the clockwise rotation of the Willamette microplate (Wells, 1990; McCaffrey et al 2000). Estimates of up to ~3 km of subsidence have been suggested within the High Cascades graben between Three Sisters and Mount Jefferson (Fig. 18; Conrey et al., 2002).

Young (<1.2 ± 0.1 Ma), behind-the-arc basaltic volcanism to the Oregon Cascades is limited to the vicinity of Newberry Volcano (Fig. 18; Jensen, 2000 and references therein). Newberry is a shield volcano situated approximately 50 km east of the axis of the High Cascades and encompasses an area of approximately 1300 km^2 (Fig. 18; Jensen, 2000). Despite its clear location in a back-arc position, the origin of Newberry Volcano with regard to the Cascadia subduction zone is difficult to interpret due to the multiple tectonic and volcanic regimes converging at its location. Newberry Volcano is situated at the intersection of the northernmost Basin and Range normal faults and the Brothers fault zone, a northwest-trending fault zone intersecting the Cascades to the north of Newberry, creating a complicated tectonic setting (Higgins, 1973; Jordan, 2001). In addition, prior studies have also suggested that Newberry Volcano is related to High Lava Plains volcanism, extending east-west across Central Oregon along the northern boundary of the Basin and Range (Jordan, 2005). However, the presence of calc-alkaline volcanics, compositionally similar to those found in the Cascades to the west, provides a basis for interpreting Newberry as a back-arc volcanic center to the Oregon Cascades, similar in regards to Medicine Lake Volcano behind-the-arc relative to Mount Shasta (Rowe et al. 2003; Kinzler et al., 2000).

Petrology and geochemistry

Previous geochemical and petrologic studies in the Oregon Cascades have potentially identified up to four distinct basaltic compositions based largely on trace-element concentrations (Bacon, 1990; Bacon et al., 1997; Conrey et al., 1997). These endmembers are commonly referred to as low-K tholeiitic basalts (also referred to as

MORB-like basalt and High Alumina Olivine Tholeiites or HAOT's), OIB-like basalts, calc-alkaline basalts, and shoshonitic basalts (including both absarokites and high-K CAB's of Conrey et al. 1997). Some ambiguity exists however regarding the distinction and classification of these compositional groups and has led to confusion in the literature.

For the purpose of this study, we will retain the LKT, OIB-like, CAB and shoshonitic nomenclature although categorization of these basalts is based dominantly on trace-element characteristics (Table 7, 8; Fig. 19). In addition to geochemical characteristics, phenocryst phases and groundmass textures between basalt groups are also distinctive. Calc-alkaline basalts are dominated by both olivine and plagioclase phenocrysts whereas OIB-like basalts have olivine phenocrysts with olivine + plagioclase in the groundmass. The phenocryst assemblage of shoshonitic basalts ranges from olivine and clinopyroxene in mafic compositions to olivine and plagioclase in slightly more evolved compositions. Trace fluor-phlogopite and fine-grained apatite phenocrysts have also been identified in shoshonitic basalts. Low-K tholeiitic lavas are distinguished by a diktytaxitic texture with plagioclase + olivine ± clinopyroxene.

Distribution of basalts

The majority of the arc volcanism has been restricted to within the confines of the intra-arc graben structure for at least the past 5 million years. Basaltic compositions of all of the previously discussed types are observed within the graben over a distance of less than 30 km across the arc (Sherrod and Conrey, in prep.). The only young forearc basalt included in this study is a shoshonitic lava located within the Western Cascade province dated at 82.3 ± 3.1 ka (Appendix E). Although a limited number of other

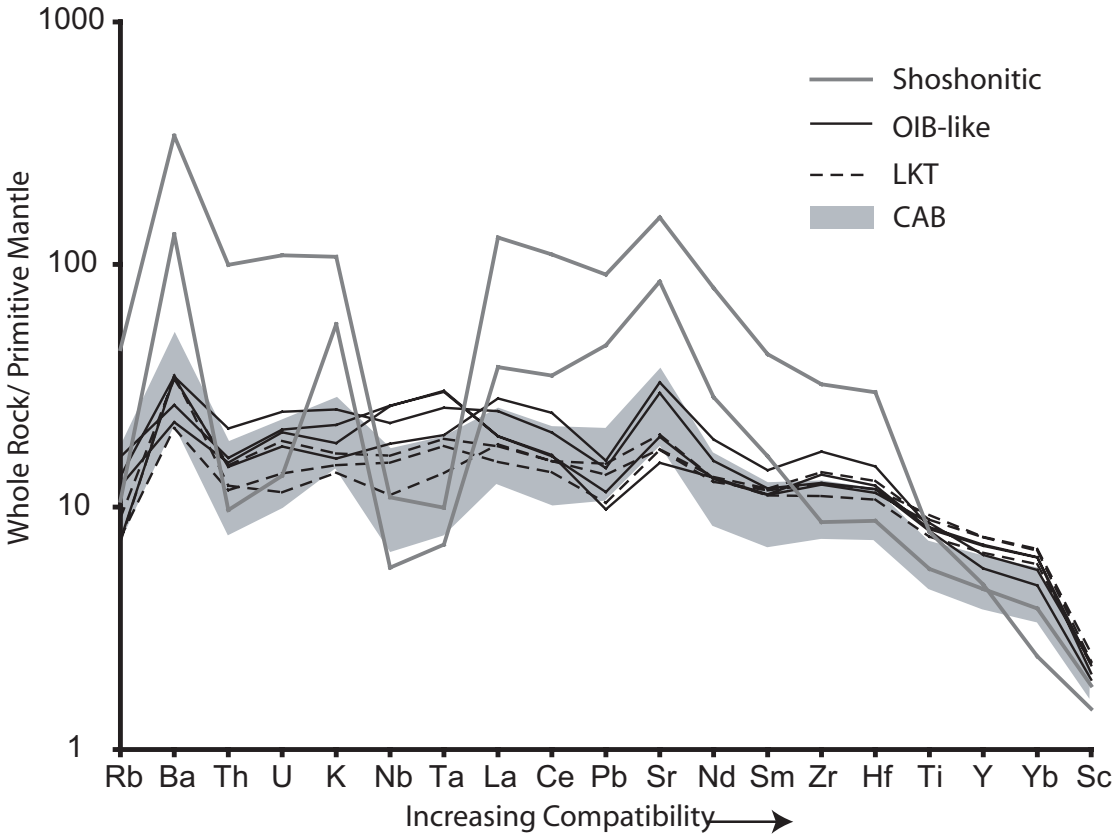

Figure 19. Primitive mantle normalized trace element diagram of basaltic whole rock compositions included in this study, depicting geochemical variations between basalt groups (McDonough and Sun, 1995). Shaded field represents the compositional range of calc-alkaline basalts. Basalts are classified based largely on their trace element concentrations and ratios (see Table 7).

Table 7: Geochemical characteristics of basalt groups

Group	K_2O wt%[2]	MgO wt%	$(K/Nb,Ta)_N$[1]	$(Ce/Pb)_N$[1]	Other Characeristics
Shoshonitic	>1.6	>9.0	>>1	Variable	Enriched in LILE, LREE, MREE; depleted in HREE, some HFSE
CAB	0.47-0.84	5.80-9.97	>1	<1	Enriched in LILE
LKT	0.40-0.48	6.81-9.03	~1	~1	Slight Ba and Sr enrichment
OIB-like	0.46-0.73	8.52-9.49	<1	>1	Enriched in Ba, Sr, HFSE, REE

Notes: [1]Normalized to primitive mantle (McDonough and Sun, 1995). [2]CAB and OIB-like basalts are not distinguishable based on K_2O wt% alone.

Table 8: Whole rock and average melt inclusion major and trace element compositions.

Sample	LL-02-1		DB-04-2		CC-02-1		BC-02-1		BR-04-2	
Latitude	44.437	Inclusion	43.804	Inclusion	44.059	Inclusion	44.014	Inclusion	43.605	Inclusion
Longitude	-121.9195	Average	-121.6543	Average	-121.7127	Average	-121.6991	Average	-121.3783	Average
Distance (Km)[1]	269	(14/1)[3,4]	282	(12/4)	287	(50/12)	288	(34/7)	305	(20/4)
Group	CAB		CAB		CAB		CAB		CAB	
Major element analysis (wt%)[2]										
SiO_2	50.42	48.10	50.13	50.51	51.94	50.10	50.85	48.42	51.73	49.34
TiO_2	1.43	1.36	1.29	1.41	1.05	1.07	1.34	1.33	1.25	1.32
Al_2O_3	16.76	15.79	17.23	17.88	16.53	17.92	17.18	17.42	16.91	17.12
FeO*	8.39	11.18	8.66	9.36	7.85	8.58	8.21	11.10	8.22	9.53
MnO	0.15	0.12	0.15	0.15	0.15	0.13	0.16	0.15	0.15	0.15
CaO	9.26	9.46	9.06	9.46	9.15	9.94	9.33	9.03	9.04	9.97
MgO	8.48	9.42	7.82	7.18	8.62	8.00	8.03	8.22	7.09	8.56
K_2O	0.82	0.77	0.53	0.55	0.65	0.62	0.62	0.55	0.84	0.49
Na_2O	3.26	3.12	3.40	2.96	3.13	3.24	3.38	3.20	3.27	3.07
P_2O_5	0.36	0.40	0.27	0.29	0.22	0.21	0.28	0.30	0.22	0.24
S	--	0.13	--	0.09	--	0.10	--	0.10	--	0.09
Cl	--	0.06	--	0.03	--	0.06	--	0.03	--	0.03
Total	99.33	99.91	98.54	99.87	99.30	99.95	99.37	99.85	98.72	99.90
Fe^{3+}/Fe_{tot}	--	0.17	--	0.18	--	0.17	--	0.19	--	0.17
Host Fo#	--	85.9	--	84.7	--	86.9	--	84.5	--	86.5
Trace element analysis (ppm)[2]										
La	16.59	19.3	9.97	10.3	10.01	8.3	11.32	11.0	10.65	7.5
Ce	36.00	51.1	22.27	27.8	21.31	21.2	25.00	28.4	23.07	21.1
Pr	4.67	6.6	2.97	3.7	2.76	2.7	3.30	3.7	3.03	2.7
Nd	20.79	26.8	14.12	16.0	12.48	11.7	15.18	17.0	14.15	11.9
Sm	5.15	6.9	4.07	3.8	3.39	3.4	4.24	4.3	4.08	2.9
Eu	1.72	1.6	1.41	1.5	1.23	1.2	1.50	1.6	1.38	1.2
Gd	5.01	6.7	4.29	4.4	3.66	3.5	4.52	5.1	4.39	3.4
Tb	0.79		0.74		0.61		0.77		0.77	
Dy	4.63	4.3	4.55	4.6	3.77	3.2	4.73	4.5	4.81	3.1
Ho	0.95		0.91		0.78		0.98		0.97	
Er	2.52	2.9	2.53	2.3	2.10	2.0	2.66	2.8	2.73	2.0
Tm	0.36		0.36		0.30		0.37		0.39	
Yb	2.20	1.9	2.23	2.4	1.84	1.9	2.37	2.8	2.44	1.9
Lu	0.34		0.35		0.29		0.37		0.39	
Ba	354	433	201	212	224	206	207	211	249	188
Th	1.49	2.4	0.64	0.7	1.27	1.3	1.07		1.75	0.7
Nb	11.50	17.6	6.91	7.8	6.67	7.3	8.07	9.6	8.03	7.8
Y	25.07	26.8	24.68	25.2	20.49	19.8	25.72	27.3	26.43	18.7
Hf	3.33	4.1	2.86		2.41	2.5	2.99	3.4	3.13	1.8
Ta	0.72	1.1	0.43	0.4	0.42	0.4	0.54	0.6	0.55	0.4
U	0.46		0.25	0.3	0.44	0.5	0.37		0.58	0.3
Pb	3.13	6.4	2.29	3.1	2.76	2.6	2.58	3.0	2.91	2.5
Rb	9.0	11.3	7.0	7.8	10.9	10.5	9.7	9.6	18.0	8.1
Cs	0.19		0.23		0.39	0.4	0.32		0.65	0.4
Sr	743	798	402	437	431	480	414	471	378	384
Sc	29.7	25.4	29.8	28.9	31.3	32.5	31.2	29.2	29.1	26.0
Zr	135	162	117	126	93	94	123	140	118	83
V		291						231		238

Notes: [1]Distance in Km to the trench- sample FLR03-1 has been adjusted to its approximate vent location. [2]XRF and ICP-MS whole rock analyses performed at Washington State University. Accuracy and precision of analyses are discussed by Johnson et al (1999) and Knaack et al. (1994). [3]Average melt inclusion major element and trace element compositions measured by electron microprobe and LA-ICPMS, respectively, at Oregon State University. Number of analyses by EMPA/LA-ICPMS.[4]Melt inclusion compositions are recalculated to be in equilibrium with their host olivine (see text).

Table 8: Continued

Sample	BB-03-1		KWB-03-1		LTB-02-1		AIC-02-1		TB-02-1	
Latitude	43.931	Inclusion	43.815	Inclusion	43.874	Inclusion	43.906	Inclusion	43.592	Inclusion
Longitude	-121.2629	Average	-121.2547	Average	-121.2178	Average	-121.159	Average	-121.1498	Average
Distance (Km)[1]	312	(22/2)	314	(17/3)	316	(33/3)	321	(26/6)	323	(38/6)
Group	CAB		CAB		CAB		CAB		CAB	
Major element analysis (wt%)[2]										
SiO_2	49.39	50.35	52.20	52.27	51.13	50.17	49.13	50.14	51.77	50.09
TiO_2	1.34	1.65	0.98	1.42	1.23	1.33	1.34	1.44	0.92	1.45
Al_2O_3	17.24	17.02	18.94	17.09	17.57	18.62	17.22	18.42	17.00	18.33
FeO*	9.16	10.76	7.03	9.93	8.06	8.49	8.76	8.20	7.66	7.90
MnO	0.16	0.16	0.12	0.15	0.15	0.13	0.15	0.12	0.13	0.10
CaO	9.58	9.23	9.74	8.25	9.54	10.17	9.86	10.73	8.55	10.22
MgO	8.17	5.74	5.80	5.35	8.16	6.39	8.43	6.51	9.97	7.76
K_2O	0.53	0.75	0.64	0.90	0.57	0.59	0.47	0.52	0.60	0.59
Na_2O	3.24	3.52	3.34	3.87	3.26	3.57	3.08	3.41	3.04	3.06
P_2O_5	0.27	0.43	0.20	0.41	0.28	0.32	0.26	0.31	0.18	0.30
S	--	0.12	--	0.11	--	0.10	--	0.12	--	0.09
Cl	--	0.04	--	0.05	--	0.03	--	0.03	--	0.05
Total	99.07	99.77	98.99	99.80	99.95	99.90	98.70	99.93	99.82	99.94
Fe^{3+}/Fe_{tot}	--	0.28	--	0.29	--	0.20	--	0.19	--	0.16
Host Fo#	--	81.5	--	82.0	--	85.0	--	85.6	--	87.4
Trace element analysis (ppm)[2]										
La	8.70	11.3	8.74	10.6	9.72	9.4	8.99	8.2	8.10	8.7
Ce	20.02	31.1	18.39	28.2	21.22	25.6	20.20	23.2	17.24	22.9
Pr	2.78	4.1	2.41	3.5	2.85	3.1	2.74	3.1	2.21	3.1
Nd	13.66	18.5	11.24	15.2	13.31	13.8	13.11	13.6	10.38	13.0
Sm	4.12	4.6	3.12	3.4	3.78	3.4	3.81	3.6	2.81	3.0
Eu	1.46	1.6	1.11	1.2	1.39	1.3	1.41	1.1	1.04	1.0
Gd	4.61	4.8	3.31	3.6	4.15	3.8	4.16	3.4	3.01	3.1
Tb	0.81		0.55		0.68		0.72		0.50	
Dy	5.11	4.7	3.42	3.8	4.16	3.7	4.50	3.8	3.09	2.9
Ho	1.06		0.70		0.85		0.93		0.61	
Er	2.89	2.8	1.83	1.9	2.25	2.0	2.55	2.1	1.67	1.8
Tm	0.41		0.26		0.33		0.37		0.24	
Yb	2.57	2.8	1.61	1.7	2.00	1.9	2.27	2.0	1.47	1.6
Lu	0.40		0.25		0.31		0.34		0.23	
Ba	169	312	260	344	236	260	178	192	238	258
Th	0.89	1.4	1.05	1.2	0.75	0.7	0.72	0.6	0.85	1.0
Nb	5.37	8.5	4.54	7.1	7.29	8.8	7.77	8.7	4.31	6.7
Y	28.25	29.3	18.31	21.1	22.32	20.2	24.55	22.4	16.41	18.1
Hf	3.00	2.8	2.18	2.1	2.43	2.1	2.58	2.3	2.03	2.0
Ta	0.33	0.4	0.29	0.4	0.47	0.5	0.51	0.5	0.28	0.4
U	0.32	0.7	0.40	0.6	0.31	0.3	0.28	0.3	0.33	0.5
Pb	2.11	4.2	3.01	4.1	2.46	2.9	1.97	2.4	2.76	3.5
Rb	7.6	18.0	9.8	14.7	7.2	7.5	6.5	7.2	8.2	12.3
Cs	0.24	0.6	0.35	0.5	0.23		0.19	0.4	0.29	0.5
Sr	357	469	541	487	453	468	400	398	460	433
Sc	30.3	29.0	26.3	23.9	30.1	29.9	32.6	34.7	25.3	22.8
Zr	118	129	81	100	95	96	104	102	76	89
V										

Table 8: Continued

Sample	SIC-02-1		ELK-02-1		FLR-03-1		BYC-02-1		NEF-03-1	
Latitude	43.583	Inclusion	44.083	Inclusion	44.172	Inclusion	43.934	Inclusion	43.821	Inclusion
Longitude	-121.0785	Average	-121.064	Average	-122.1061	Average	-121.1916	Average	-121.0953	Average
Distance (Km)[1]	329	(23/3)	339	(8/3)	275	(23/4)	318	(7/0)	326	(18/5)
Group	CAB		CAB		LKT		LKT		LKT	
Major element analysis (wt%)[2]										
SiO_2	49.81	49.72	49.39	48.65	49.08	47.71	49.77	47.17	48.89	48.75
TiO_2	1.26	1.36	1.21	1.55	1.51	1.75	1.77	1.92	1.85	2.02
Al_2O_3	17.19	18.55	17.95	17.11	16.94	17.51	17.10	17.43	16.83	17.14
FeO*	8.82	8.55	8.57	11.59	9.57	10.93	10.62	13.33	10.14	10.68
MnO	0.16	0.14	0.15	0.18	0.18	0.16	0.19	0.20	0.18	0.18
CaO	9.84	10.59	9.88	9.38	9.83	10.47	9.41	9.35	10.63	10.47
MgO	8.69	7.15	8.75	6.68	9.03	7.82	6.81	5.69	6.82	6.02
K_2O	0.48	0.41	0.50	0.73	0.40	0.45	0.48	0.54	0.43	0.54
Na_2O	3.03	3.09	3.03	3.39	3.07	2.53	3.44	3.47	3.37	3.46
P_2O_5	0.19	0.24	0.24	0.38	0.33	0.35	0.33	0.35	0.33	0.38
S	--	0.09	--	0.12	--	0.11	--	0.14	--	0.15
Cl	--	0.03	--	0.04	--	0.03	--	0.02	--	0.03
Total	99.46	99.91	99.66	99.81	99.94	99.82	99.92	99.62	99.47	99.82
Fe^{3+}/Fe_{tot}	--	0.18	--	0.25	--	0.20	--	0.35	--	0.26
Host Fo#	--	85.3	--	82.2	--	84.1	--	79.4	--	82.0
Trace element analysis (ppm)[2]										
La	7.03	5.2	8.06	10.0	11.77	8.9	11.57		9.96	9.7
Ce	16.13	15.9	17.98	24.8	25.95	25.4	25.98		23.35	28.5
Pr	2.24	2.2	2.46	3.2	3.58	3.4	3.48		3.24	3.6
Nd	10.85	9.8	12.00	13.5	16.37	15.3	16.62		15.87	16.2
Sm	3.42	2.4	3.58	4.3	4.58	3.6	4.88		4.81	4.2
Eu	1.28	1.1	1.30	1.6	1.64	1.5	1.79		1.74	1.5
Gd	3.85	3.1	3.98	8.4	4.95	4.1	5.45		5.58	5.9
Tb	0.69		0.67		0.82		0.97		0.98	
Dy	4.37	3.0	4.23	4.7	5.18	4.3	6.00		6.12	4.7
Ho	0.89		0.87		1.05		1.21		1.25	
Er	2.44	2.0	2.36	3.0	2.88	2.4	3.32		3.39	2.9
Tm	0.35		0.34		0.40		0.49		0.48	
Yb	2.12	1.9	2.09	2.8	2.56	2.9	2.90		2.95	2.3
Lu	0.34		0.33		0.40		0.46		0.46	
Ba	154	134	215	379	231	286	223		140	159
Th	0.96	0.5	0.74	1.1	0.98	1.2	1.19		0.94	0.9
Nb	5.21	5.0	5.43	7.8	7.39	9.0	10.75		10.05	10.8
Y	23.49	19.3	23.24	29.1	27.82	26.5	32.25		32.39	31.6
Hf	2.37	1.5	2.51	3.6	3.00	1.7	3.58		3.32	
Ta	0.35	0.3	0.35		0.51	0.6	0.71		0.66	0.6
U	0.34	0.2	0.29	0.4	0.23	0.4	0.37		0.28	0.4
Pb	3.03	1.7	1.90	1.7	2.27	2.8	2.04		1.56	2.1
Rb	7.7	6.2	6.5	18.1	4.3	9.7	5.4		4.5	9.8
Cs	0.29		0.20		0.20		0.13		0.09	
Sr	341	347	369	327	398	395	346		344	314
Sc	33.7	27.9	27.0	61.5	35.7	27.7	37.0		39.8	38.6
Zr	87	71	99	135	116	120	146		131	138
V				185		267				

Table 8: Continued

Sample	HL-03-1		WF-04-1		NMB-03-1		BLW-03-1		QV-03-1	
Latitude	44.782	Inclusion	44.491	Inclusion	43.841	Inclusion	43.511	Inclusion	44.600	Inclusion
Longitude	-121.7771	Average	-121.6259	Average	-121.286	Average	-120.8617	Average	-122.3369	Average
Distance (Km)[1]	279	(8/2)	292	(28/8)	311	(7/0)	347	(43/11)	237	(41/9)
Group	OIB		OIB		OIB		OIB		SHO	
Major element analysis (wt%)[2]										
SiO_2	49.48	46.89	48.50	48.56	48.11	47.61	47.84	47.61	50.06	49.67
TiO_2	1.60	2.05	1.65	1.93	1.72	2.08	1.62	1.65	1.58	1.68
Al_2O_3	16.23	17.89	15.52	18.70	16.36	17.64	16.49	17.22	13.64	14.99
FeO*	8.88	9.51	10.47	7.57	9.64	9.31	9.89	9.91	6.53	6.82
MnO	0.15	0.13	0.18	0.12	0.16	0.15	0.17	0.16	0.11	0.10
CaO	9.50	12.12	9.17	11.61	10.32	12.18	10.11	10.39	10.14	9.85
MgO	8.71	6.13	9.49	6.78	8.52	6.08	8.99	8.78	9.86	6.77
K_2O	0.73	0.72	0.46	0.52	0.63	0.45	0.53	0.51	3.11	2.17
Na_2O	3.32	3.77	2.88	3.51	3.11	3.30	3.04	3.18	2.88	2.49
P_2O_5	0.33	0.41	0.49	0.51	0.31	0.90	0.35	0.36	1.17	1.33
S	--	0.12	--	0.13	--	0.10	--	0.11	--	0.37
Cl	--	0.09	--	0.14	--	0.03	--	0.03	--	0.15
Total	98.93	99.81	98.82	100.07	98.88	99.83	99.04	99.91	99.07	96.40
Fe^{3+}/Fe_{tot}	--	0.24	--	0.18	--	0.23	--	0.17	--	0.31
Host Fo#	--	84.3	--	86.6	--	83.6	--	86.3	--	89.2
Trace element analysis (ppm)[2]										
La	16.16	17.6	18.24	19.6	12.71		12.74	12.3	83.94	94.9
Ce	34.07	55.5	41.07	54.7	27.19		27.53	31.0	184.60	262.8
Pr	4.35	6.3	5.34	6.9	3.49		3.54	3.9	24.35	32.0
Nd	19.37	27.5	23.74	27.9	16.33		16.51	16.6	100.09	123.5
Sm	4.89	6.4	5.81	5.6	4.60		4.62	4.6	17.49	19.6
Eu	1.68	1.9	1.93	1.9	1.63		1.62	1.4	4.59	4.7
Gd	4.80	4.3	5.88	6.1	4.91		5.10	5.0	10.35	10.5
Tb	0.78		0.93		0.83		0.88		1.11	
Dy	4.64	6.2	5.67	5.7	5.21		5.49	5.4	4.85	4.2
Ho	0.93		1.15		1.05		1.14		0.74	
Er	2.46	2.4	3.07	3.3	2.77		3.06	3.1	1.64	1.5
Tm	0.34		0.44		0.39		0.44		0.20	
Yb	2.09	2.2	2.73	2.9	2.42		2.72	2.8	1.07	1.3
Lu	0.32		0.44		0.37		0.44		0.16	
Ba	227	269	226	241	174		148	152	2242	2802
Th	1.69	2.2	1.17	1.1	1.28		1.22	1.7	7.97	9.6
Nb	14.64	18.6	12.03	13.5	17.26		17.22	20.0	7.23	9.0
Y	24.01	30.9	30.05	33.8	27.29		29.72	29.6	20.60	20.4
Hf	3.32	4.3	4.11	5.3	3.20		3.43	2.9	8.31	
Ta	0.95	1.3	0.73	0.8	1.10		1.11	1.1	0.37	0.4
U	0.49		0.36	0.5	0.42		0.41	0.7	2.18	3.4
Pb	2.17	3.1	2.33	3.4	1.73		1.47	1.8	13.63	22.2
Rb	8.0	9.4	4.4	4.2	9.7		7.3	8.5	26.9	45.9
Cs	0.06		0.15	2.5	0.18		0.13		0.20	
Sr	591	677	653	1045	389		304	324	3124	3975
Sc	31.0	27.3	33.0	37.9	36.5		35.6	34.7	23.5	19.2
Zr	132	183	178	224	130		143	157	336	372
V		391						235		

Table 8: Continued

Sample	CM-02-2	
Latitude	44.361	Inclusion
Longitude	-121.7619	Average
Distance (Km)[1]	282	(77/15)
Group	SHO	
Major element analysis (wt%)[2]		
SiO_2	50.27	48.68
TiO_2	1.11	1.30
Al_2O_3	16.44	18.29
FeO*	7.48	7.20
MnO	0.14	0.10
CaO	9.77	11.50
MgO	9.06	7.23
K_2O	1.64	1.96
Na_2O	2.95	3.09
P_2O_5	0.39	0.48
S	--	0.18
Cl	--	0.08
Total	99.25	100.10
Fe^{3+}/Fe_{tot}	--	0.16
Host Fo#	--	87.7
Trace element analysis (ppm)[2]		
La	24.55	28.8
Ce	58.46	81.7
Pr	8.12	11.4
Nd	35.48	48.4
Sm	6.64	7.8
Eu	2.09	2.5
Gd	4.79	5.5
Tb	0.67	
Dy	3.83	4.0
Ho	0.74	
Er	1.91	2.0
Tm	0.27	
Yb	1.68	2.0
Lu	0.26	
Ba	879	1140
Th	0.78	0.9
Nb	3.71	3.8
Y	19.74	22.8
Hf	2.46	3.0
Ta	0.26	0.3
U	0.27	0.4
Pb	6.96	10.4
Rb	6.4	5.6
Cs	0.15	3.3
Sr	1701	2166
Sc	29.3	28.1
Zr	91	116
V		

relatively young calc-alkaline basalts are present in the forearc they have been dated at ~3Ma and outside the range of the current study (Walker and Duncan, 1989).

Young backarc volcanism along the Cascade volcanic arc is limited to three general locations; Simcoe volcanic field in southern Washington, Newberry Volcano in central Oregon, and Medicine Lake in northern California (Fig. 18). Similar to the High Cascades, basaltic compositions at Newberry Volcano are highly variable. Although CAB's are the dominant basaltic composition at Newberry, both OIB-like and LKT lavas are found around the flanks of the volcano. Young shoshonitic compositions have not been identified in the backarc region at Newberry Volcano. As a result of the abundant young volcanism around Newberry Volcano, in conjunction with High Cascade and forearc lavas, primitive basalt compositions corresponding to the distinct compositional endmembers can be examined from over 100 km across the Cascade volcanic arc.

METHODS

Sample collection

High Cascade basalts utilized in this study were selected based age (< 1 Ma), location (43-45°N), and composition from a geochemical database for the Oregon Cascades provided by R. Conrey (Conrey et al., 1997; Sherrod and Conrey, in prep). Newberry backarc basalts were selected based on previous whole rock geochemical studies to provide the most primitive samples available (Linneman, 1990, Jordan, 2001, Beyers, 1973, Higgins, 1973, MacLeod et al., 1995; MacLeod and Sherrod, 1988). High Cascades and forearc basalt samples in this study have greater than 8 wt% MgO and

backarc basalts have greater than 6 wt% MgO and all basalt samples are olivine bearing (Table 8). Whole rock major and trace elements concentrations for basalts in this study were measured by XRF and ICP-MS, respectively, at the Washington State University geochemical lab. Samples were specifically targeted between 45°N and 43°N to provide the greatest compositional range representative of the four previously identified endmembers while reducing the possibility for along arc compositional variations (Fig. 18; Conrey et al. 1997). Samples of lava and scoria were collected from vent or near vent localities when possible, however due to the rapid burial of lavas and erosion, resulting in the loss of vent material, more distal lavas had to be collected in some cases.

Sample preparation and rehomogenization

Lava and scoria samples were lightly crushed and olivine grains handpicked. Olivine grains were examined in ethanol under a binocular microscope to determine if rehomogenization was required. In most cases melt inclusions in olivine grains were found to be partially (<5%) to completely crystalline, requiring rehomogenization. Melt inclusions were rehomogenized in an atmosphere-controlled Deltec 1 atm vertical furnace following the procedure described by Rowe et al (2006). Inclusions were held at near-liquidus temperatures estimated from bulk rock compositions for ~10 minutes to ensure rehomogenization, then rapidly quenched. Samples were held at high temperatures for a maximum of 10-15 minutes to reduce the potential for hydrogen diffusion (Danyushevsky et al., 2002; Hauri, 2002). Oxygen fugacity within the furnace was maintained at the Fayalite-Magnetite-Quartz (FMQ) oxygen buffer with a mixture of CO_2 and H_2 gas. Following rehomogenization, olivine grains were mounted in 25 mm